Identification of efficient promoters and selectivity trends in high temperature Fischer-Tropsch synthesis over supported iron catalysts

Alan Barrios, Bang Gu, Yuan Luo, Deizi Peron, Petr. Chernavskii, Mirella Virginie, Robert Wojcieszak, Joris W Thybaut, Vitaly Ordomsky, Andrei Khodakov

Draft March 31st, 2020

Identification of efficient promoters and selectivity trends in high temperature Fischer-Tropsch synthesis over supported iron catalysts

*Alan J. Barrios[a], Bang Gu[a], Yuan Luo[a], Deizi V. Peron[a], Petr. A. Chernavskii[b], Mirella Virginie[a], Robert Wojcieszak[a], Joris W. Thybaut[c], Vitaly V. Ordomsky[a] and Andrei Y. Khodakov[a]**

[a]*Univ. Lille, CNRS, Centrale Lille, ENSCL, Univ. Artois, UMR 8181 – UCCS – Unité de Catalyse et Chimie du Solide, F-59000 Lille, France.*

[b]*Department of Chemistry, Moscow State University, 119992 Moscow, Russia*

[c]*Laboratory for Chemical Technology (LCT), Department of Materials, Textiles and Chemical Engineering, Ghent University, Technologiepark 125, 9052 Ghent, Belgium.*

Corresponding author:andrei.khodakov@univ-lille.fr

Abstract

In this work, 29 elements were evaluated as promoters for silica supported iron catalysts for high temperature Fischer-Tropsch using a high-throughput experimentation unit. The selected promoters include alkali/alkaline metals, transition metals, precious metals and lanthanides. Several general selectivity trends were observed and discussed. The selectivity enhancement to light olefins requires maintaining low selectivity to methane and light paraffins and at the same time, slowing the chain growth to the C_{5+} hydrocarbons.

A major increase in Fischer-Tropsch rate principally due to higher intrinsic site activity, was observed over the catalysts promoted with metals with low melting points such as tin, antimony, bismuth and lead. These promoted catalysts also exhibited better stability. The effect of the promotion with tin and antimony on the olefin selectivity was not noticeable, while the presence of bismuth and lead results in the major enhancement of the selectivity to light olefins, lower methane and C_2-C_4 paraffin selectivities.

Keywords: renewable fuels; Fischer-Tropsch; iron catalysts; promotion; high throughput; light olefins

Introduction

The interest in high temperature Fischer-Tropsch (FT) synthesis has been growing in the last decades, because this reaction provides an opportunity for conversion of alternative and renewal feedstocks [1,2], such as biomass, organic and plastic waste, into value-added chemicals such as light olefins. In addition, FT synthesis produces ultra clean and environmentally friendly chemicals, which are essentially free from sulfur, nitrogen and undesirable aromatics. Iron catalysts have shown the highest activity and olefin selectivity in FT synthesis [3–6]. In recent years, the research interests have shifted from bulk to supported iron FT catalysts. Indeed, supported iron catalysts provide higher surface area and iron dispersion, more efficient use of active phase and promoters, better mechanical resistance and potentially enhanced activity, selectivity and stability. The catalytic performance of supported iron catalysts can be further improved by several strategies such as promotion [7,8], nanoconfinement [9–11] of active phase and by optimization of the interaction of iron species with the support [12].

The FT reaction involves iron carbide species [13–17], which form in-situ in the iron catalysts during activation in carbon monoxide or syngas. FT synthesis is a complex catalytic reaction; in addition to iron carbide, the presence of different iron oxide species and metallic iron can affect the overall catalytic performance [18,19]. Electronic and structural promoters have been intensively used in order to increase iron dispersion, extent of iron carbidisation, FT reaction rates and light olefin selectivity over Fe-based catalysts. Addition of promoters can affect iron dispersion, iron carbidisation, electronic properties of the active species and rate of primary and secondary elementary steps of FT synthesis. Most of earlier publications have been focused on the promotion of iron catalysts with alkali metals [7,20–26] and copper [7,25,27,28]. More recently, the group of de Jong [3,29,30] and Sasol researchers [31] reported that simultaneous addition of sodium and sulfur improved the selectivity to olefins.

Note however, that promoter effect on the FT reaction selectivity over iron catalysts is rather complex, since the rate of several FT elementary steps could be affected. In many cases, direct comparison of iron catalysts promoted with different elements is not obvious, because of different supports, promoter content, catalyst preparation and activation procedures. Very few information is available in the literature about influence of the promoters on the catalytic performance of iron catalysts on the same support, prepared using the same method, at the same concentration level and tested under exactly the same reaction conditions. Recently, we have discovered [10,11,32,33] that the catalytic performance of iron catalysts can be significantly improved by using bismuth or lead as promoters; the reaction rate was increased several times over the promoted catalysts.

High throughput experimentation (HTE) [31–33] represents nowadays a powerful tool for the design of new efficient heterogeneous catalysts. The goal of this paper is to explore the potential of HTE for identification of efficient promoters and selectivity trends in FT synthesis. The conducted experiments cover numerous promoters from 1A-5A and 1B-8B groups of the Periodic Table, which include alkali/alkaline metals, transition metals, precious metals and lanthanides for iron FT catalysts. 29 elements (Li, K, Cs, Mg, Ca, Sr, Ba, La, Ce, Zr, Nb, Cr, Mo, W, Mn, Co, Ni, Pd, Cu, Ag, Au, Zn, Ga, In, Sn, Pb, P, Sb, Bi) at the same molar concentration in the catalyst were evaluated in high temperature FT synthesis. For the best of our knowledge, it is the first time that such amount of promoters has been systematically evaluated under the same reaction conditions. Thanks to high-throughput experimental unit, we identified new promoters (Sn and Sb) able to improve activity of iron-based catalysts even when using small quantities of them. Furthermore, these new efficient promoters were never tested for FT synthesis. Silica is a common support for many heterogeneous catalysts and has been widely used in numerous industrial applications. The supported iron catalysts were prepared by incipient wetness impregnation of silica with

aqueous solutions of hydrous iron nitrate. The catalytic results and in particular those relevant to the selectivity and stability were measured as a function of carbon monoxide conversion. They are compared and discussed with those obtained for the reference non-promoted iron catalyst.

2. Experimental

2.1 Catalyst preparation

Commercial amorphous silica (CARIACT Q-10, Fuji Silesia) was used as the catalytic support. The textural properties of the support are given in **Table S1, Supplementary Information (SI).** Generally, distilled water is served as solvent. In the case of Nb and Sb, ethanol (Verbiese) is applied as to the insolubility of Nb and Sb salts in water. The following precursors were used for the promotion of silica supported iron catalysts: $LiNO_3$ (Fluka), KNO_3 (Sigma-Aldrich), $CsNO_3$ (Aldrich), $Mg(NO_3)_2.6H_2O$ (Sigma-Aldrich), $Ca(NO_3)_2.4H_2O$ (Sigma-Aldrich), $Sr(NO_3)_2$ (Sigma-Aldrich), $Ba(NO_3)_2$ (Sigma-Aldrich), $La(NO_3)_3.6H_2O$ (Fluka), $Ce(NO_3)_3.6H_2O$ (Fluka), $ZrO(NO_3)_2 \cdot xH_2O$ (Fluka), $NbCl_5$ (Alfa Aesar), $Cr(NO_3)_3.9H_2O$ (Sigma-Aldrich), $(NH_4)_6Mo_7O_{24} \cdot 4H_2O$ (Fluka), $(NH_4)_{10}(H_2W_{12}O_{42}) \cdot xH_2O$ (Aldrich), $Mn(NO_3)_2.4H_2O$ (Alfa Aesar), $Co(NO_3)_2.6H_2O$ (Sigma-Aldrich), $Ni(NO_3)_2.6H_2O$ (Sigma-Aldrich), $Pd(NO_3)_2.xH_2O$ (Aldrich), $Cu(NO_3)_2.3H_2O$ (Acros Organics), $AgNO_3$ (Sigma-Aldrich), $HAuCl_4$ (Aldrich), $Zn(NO_3)_2.6H_2O$ (Sigma-Aldrich), $Ga(NO_3)_3.xH_2O$ (Sigma-Aldrich), $In(NO_3)_3.xH_2O$ (Sigma-Aldrich), $SnCl_2 \cdot 2H_2O$ (Sigma-Aldrich), $Pb(NO_3)_2$ (Sigma-Aldrich), $(NH_4)_2HPO_4$ (Sigma-Aldrich), $SbCl_3$ (Sigma-Aldrich), $Bi(NO_3)_3.5H_2O$ (Sigma-Aldrich), ammonium thiosulfate (Alfa Aesar)

Except for the Sb-promoted iron catalysts, all the other promoted catalysts were prepared by single-step co-incipient wetness impregnation. The Fe catalysts promoted with Sb were synthetized twice via alternating the impregnation sequence. In first case, silica was

impregnated first with the Fe precursor and then with Sb. It gave the $SbFe/SiO_2$ sample. In the second case, silica was impregnated first with Sb and then with Fe. The $FeSb/SiO_2$ catalyst was obtained. The concentrations of the impregnating solutions were calculated in order to obtain about 10 wt. % iron in the final catalysts, the ratio of Fe to promoter (M) was 100:2. After the impregnation, the catalysts were dried overnight in an oven at 100 °C. Then they were calcined in air at 400 °C for 6 h with the 1 °C/min temperature ramping.

2.2 Catalyst characterization

The ex situ X-ray powder diffraction (XRD) experiments were conducted using a Bruker AXS D8 diffractometer with Cu Kα radiation (λ = 0.1538 nm). The XRD patterns were collected in the 20–70° (2θ) range, with the 0.02° step size and 0.5 s step time. The identification was carried out by comparison with the JCPDF standard spectra software. The average crystallite size of Fe_2O_3 or iron carbides was calculated using the diffraction peaks according to the Scherrer equation.

Relative content of oxide was determined with the use of an energy dispersive micro-X-ray Fluorescence spectrometer M4 TORNADO (Bruker). This instrument is equipped with 2 anodes: a Rhodium X-ray tube 50 kV/600 mA (30 W) and a Tungsten X-Ray tube 50 kV/700 mA (35 W). For sample characterization, the X-rays Rhodium with a polycapillary lens enabling excitation of an area of 200 μm was used. The detector used was a Silicon-Drift-Detector Si(Li) with <145 eV resolution at 100000 cps (Mn Kα) and cooled with a Peltier cooling (253°K). The measurement was done under vacuum (20 mbar). The elements, that can be measured by this instrument unit range from sodium (Na) to uranium (U). Quantitative analysis was done using fundamental parameter (FP) (standardless). The quantification was made based on the identified element.

The H_2 temperature-programmed reduction (H_2-TPR) experiments were carried out using the AutoChem II 2920 apparatus (Micromeritics) using 0.05 g of the sample in a flow of H_2/Ar (5 vol. % H_2) stream (30 ml/min). The temperature was increased from room temperature to 900 °C at the rate of 10 °C/min. The 5 vol.% H_2/Ar gas for TPR analysis was dehydrated using a trap filled with molecular sieves.

The magnetic characterization was performed using a Föner vibrating-sample magnetometer [37–39] equipped with an in-situ cell. 0.01g of the sample was placed in the in-situ cell and heated to 350 °C under the flow of pure CO (0.3°C/min, V_{CO}=30 ml/min). After reaching 350°C, the samples were kept in the flow of CO until reaching a constant value of magnetisation. After the activation, the sample was cooled to the room temperature in the flow of CO. The pre-treatment with syngas (H_2/CO=1, V_{syngas}=30 ml/min) was performed with the samples already activated in CO and using similar procedure as pre-treatment in CO. The thermomagnetic curves (magnetisation versus temperature) were measured during cooling down the catalyst in syngas from 350°C to room temperature.

2.3 Catalytic tests

The catalytic tests were carried out in the high throughput experimentation unit (HTE, Flowrence, Avantium) and in a laboratory fixed-bed reactor. In the HTE unit, the feed gas is homogeneously split by calibrated high pressure-drop capillaries into 16 reactors. Each four reactors formed one independent block, where the temperature can be separately controlled. High boiling point product (liquid phase) is constantly collected at 60 °C, before the rest gas phase flows through GC for analysis. Catalyst loading was completed in a stainless-steel tube with inner diameter of 2.0 mm, length of 15 cm. Both ends (height of 1.5 cm) of the reactor tube were filled with inert SiC (size of 0.105 mm), where the catalyst (amount: 100 mg; size: 50 – 150 μm) was loaded in between. Prior to FT synthesis, all catalysts were pretreated in

the CO atmosphere (5 mL/min) at 350 °C for 10 h and cooled to 180 °C. The activation procedure for silica supported iron catalysts was optimized in our earlier report [40]. After pressurized in H_2/CO (1:1) to 10 bar, temperature was stepwise (1 °C/min) increased to 350 °C. The catalytic performance was measured under five different WHSV: 3.4 L/h g_{cat} → 4.5 L/h g_{cat} → 6.75 L/h g_{cat} → 2.25 L/h g_{cat} → 1.5 L/h g_{cat}. We stayed minimum 9 hours at each space velocity. All catalysts achieved the quasi-steady state condition during the high-throughput testing. We did not see any noticeable catalyst deactivation during the catalyst screening in the high throughput unit. No liquid phase was collected within all the HTE tests over iron catalysts. The gaseous products were analyzed online using a gas chromatograph (GC). Permanent gases (He, H_2, O_2, N_2, CH_4, and CO) were separated by a Hayesep Q/molsieve column and determined by a TCD; CO_2 and C_2-C_3 hydrocarbons by a PPQ/PPQ column and TCD; C_5-C_{12} hydrocarbons by a CP-Sil5/CP-Sil5 column and FID, respectively.

The laboratory fixed-bed reactor used for FT synthesis had the inner diameter of 2 mm. Typically, 100 mg of the fresh catalyst was loaded into the stainless-steel tube. The catalysts were activated by heating up to 350 ^oC at a rate of 2 ^oC min^{-1} and dwelling at 350°C for 10 h under CO flow (10 mL min^{-1}) at atmospheric pressure. After cooling down to 180 ^oC, syngas with H_2/CO = 1/1 was introduced into the reactor. The Brooks mass flow meters were used to control the flow rates. The required reaction pressure was achieved by a back-pressure valve. Nitrogen with a flow of 1 mL min^{-1} in the syngas mix was used as an internal standard for the calculation of CO conversion. Once the pressure and flow rate have been stabilized, the temperature was raised (1^oC min^{-1}) to 350 ^oC to start the reaction. The reagents and reaction products were analyzed by a gas chromatograph (Varian CP-3800), which was equipped with a thermal conductivity detector (TCD) and a flame ionization detector (FID). A packed CTR-1 column was connected to the TCD, and a Rt-Q-PLOT capillary column was connected to the FID. Iron time yields (FTY) were expressed as moles of CO converted per gram of total

iron per second. The turnover frequency (TOF) was calculated [41,42] from the bulk density of Fe_5C_2 (ρ = 7.57 g mL^{-1}) and surface density of 14 Fe atoms nm^{-2}. TOF was calculated assuming the Fe_5C_2 active site [42]. The CO_2 free hydrocarbon selectivities on carbon basis were calculated taking into account only hydrocarbon production in FT synthesis.

3. Results

3.1. Silica supported iron catalysts promoted with 29 elements

3.1.2. Conversion and reaction rate

All the catalysts were tested in high temperature FT synthesis under identical conditions (H_2/CO=1, P=10 bar, T=350 °C) in both HTE and laboratory fixed bed reactors. The carbon monoxide conversion was negligible over the Cr-, Nb-, Ga-, Pd-, Co-, In-, Mo-, Zn-promoted catalysts. All other examined catalysts presented measurable CO conversions within the tested WHSV ranges. High temperature FT synthesis over all catalytic leads to light C_2-C_4 olefins, light C_2-C_4 paraffins, methane, CO_2 and C_{5+} longer chain hydrocarbons. The carbon monoxide conversions measured at iso-WHSV= 3.4 L/g·h in the HTE unit over different promoted iron catalysts are shown in **Figure 1**. Most of the promoted Fe catalysts exhibit a CO conversion in the range of 10% - 30%, which is similar or slightly higher than the non-promoted Fe/SiO_2 counterpart (**Figure 1**). Interestingly, the Bi-, Pb-, Sn- and Sb-promoted catalysts exhibit an enhanced catalytic activity. Under the same conditions, the carbon monoxide conversion on these catalysts was much higher (30-85%). The catalytic tests in the HTE setup clearly identify Bi-, Pb-, Sn- and Sb as the most promising promoters in order to obtain iron catalysts with higher activity in FT synthesis. The catalytic results for the Sn-, Sb-, Bi- and Pb-promoted iron catalysts are presented in detail in section 3.3.

3.1.2. Selectivity trends in high temperature FT synthesis

The selectivities to CO_2, methane, C_2-C_4 light olefins, light paraffins and C_{5+} hydrocarbons for all investigated catalysts measured at different WHSV are displayed in **Figure 2** and **Figure S1, SI** and plotted as functions of carbon monoxide conversion. The selectivity to carbon dioxide (**Figure S1a, SI**) displays scattered points at low conversion. The CO_2 selectivity increases as function of conversion over all catalysts and reaches the stoichiometric value of 50% at CO conversion exceeding 30%. Carbon dioxide in FT synthesis over iron catalysts is principally produced via water gas-shift (WGS) reaction: $CO+H_2O=CO_2+H_2$. Thus, some variation of the activity of the promoted catalysts can be assigned to their different activities in WGS and FT synthesis. The CO_2 selectivity close to 50% at high CO conversion suggests that FT synthesis over iron catalysts occurs simultaneously with the WGS reaction with almost complete conversion of water by its reaction with CO:

$2nCO + nH_2 = C_nH_{2n}+nCO_2$

$2nCO+ (n+1)H_2=C_nH_{2n+2}+nCO_2$

Figure S1b, SI displays methane selectivity observed on the promoted iron catalysts as a function of conversion. Higher methane selectivities were observed at rather low carbon monoxide conversion (<10%). The methane selectivity decreases with increase in conversion and at higher conversion scatters between 5 and 15% as a function of catalyst. The lowest methane selectivity was observed over the Pb and Bi-promoted catalysts and the highest over the Sn- and Zr-promoted counterparts.

The selectivity to light olefins (**Figure 2**) also decreases as a function of carbon monoxide conversion. The maximum light olefin selectivity close to 60 % is observed at the relatively low CO conversion (< 2-3 %). Indeed, the selectivity to a specific hydrocarbon range in FT synthesis is limited by the Anderson–Schulz–Flory (ASF) statistics, which predicts the

maximum selectivity of 55% for the C_2-C_4 hydrocarbons. In this work, we observed the maximum C_2-C_4 light olefin selectivity up to 60%. Again, the bismuth and lead promoted catalysts do not follow the general trend; the light olefin selectivity is higher at the same conversion level on the Bi and Pb-containing iron catalysts than on any other counterparts. The decrease in both methane and light olefin selectivities with the carbon monoxide conversion suggests that all these compounds could be primary products of FT synthesis over iron catalysts.

Interestingly, only very slight effect of carbon monoxide conversion on the selectivity to the C_2-C_4 paraffinic hydrocarbons was observed over various promoted iron catalysts (**Figure S1c, SI**). The selectivity data scatter between 5 and 20%. Interestingly, the C_2-C_4 paraffin selectivity only slightly increases as a function of carbon monoxide conversion. Taking into account that the selectivity to light olefins decreases with the CO conversion, while the selectivity to light paraffins is only slightly affected by the conversion, one can suggest that secondary olefin hydrogenation could be only one of the main reasons responsible for the decrease in the light olefin selectivity with conversion.

Carbon monoxide conversion affects to a greater extent the C_{5+} hydrocarbon selectivity (**Figure S1c, SI**). The C_{5+} selectivity is close to zero at the CO conversions lower than 10%. It steadily increases with the CO conversion and reaches 25-30 % at the CO conversion higher than 20%. The C_{5+} selectivity remains nearly constant, when the CO conversion higher than 30%. It worth noting that the decrease in the C_2-C_4 light olefin selectivity clearly coincides with the increase in the C_{5+} selectivity.

According to Schulz [43], FT synthesis is a “non-trivial surface polymerization reaction” . Carbon monoxide adsorption over surface sites of iron catalyst results in the formation of the C_1 surface monomers, which can be produced either by direct or hydrogen-assisted CO dissociation [44,45]. The shape of the methane selectivity versus conversion curve (**Figure**

S1b, SI) suggests that methane, which is produced with high selectivity at low conversion, could form directly from the hydrogenation of the C_1 surface monomers. The shape of the selectivity versus conversion curves can also be explained from the polymerization mechanism of FT synthesis. Indeed, at very low conversions, the concentrations of adsorbed C_1 monomer is potentially insufficient for noticeable polymerization to form longer chain surface fragments and respectively longer chain hydrocarbons. This could explain lower selectivity to long chain C_{5+} hydrocarbons at lower CO conversion levels.

Oligomerization of the surface C_1 monomers results in the C_2-C_4 fragments on the catalyst surface. The C_2-C_4 surface fragments can then undergo the following reaction pathways (**Figure 3**). First, they can desorb with possible partial hydrogenation yielding light olefins. Second, they can be fully hydrogenated to yield paraffins. Finally, they can react with another C_1 surface monomer, producing longer chain fragments and hydrocarbons. Important, the experimental results (**Figure 2**) indicate that the increase in CO conversion results in decrease in the selectivity to the C_2-C_4 light olefins, increase in the selectivity to longer C_{5+} hydrocarbons, while the selectivity to the C_2-C_4 hydrocarbons is much less affected by the conversion. The scheme shown in **Figure 3** suggests that higher selectivity to light olefins requires lower selectivity to the C_{5+} hydrocarbons. Indeed, on all studied iron promoted catalysts higher carbon monoxide conversion results in the increase in the C_{5+} hydrocarbon selectivity at the expense of the light olefin selectivity. Interestingly, the light paraffin selectivity is much less affected by the conversion. This suggests that full hydrogenation of adsorbed C_2-C_4 species and olefins does not become significant with the conversion. To keep high light olefin selectivity, the selectivities to long chain C_{5+} hydrocarbons and light paraffins should be reduced in particular, at high carbon monoxide conversion.

Figure 1 indicates a major increase in FT reaction rate over the iron catalyst promoted with Sn, Sb, Bi and Pb compared to any other promoters investigated in this work. In order to

provide further insights into the enhancement of the catalytic activity on the promotion, the structure of the tin and antimony promoted catalysts was studied in detail by a combination of characterization techniques. The characterization data for tin and antimony promoted catalysts are compared with those for the bismuth and lead promoted counterparts.

3.2. Characterization of the promoted catalysts

The XRF elemental analysis data for the Sn, Sb, Bi and Pb promoted catalysts are displayed in **Table 1**. All catalysts present similar iron content (around 10 wt. %), while the Sn, Sb, Pb, and Bi promoters contents were close to 0.8 wt. %. The promoter content in the Sn- and Sb- containing catalysts tested in the laboratory fixed bed reactor was slightly higher than in those used for catalytic test in HTE unit (0.45 wt.%). **Figure 4a** shows the XRD profiles of reference iron catalyst and those co-impregnated with the Sn, Sb, Pb, and Bi promoters. All the studied calcined catalysts exhibit the characteristic diffraction peaks of hematite phase (Fe_2O_3, JCPDS13-0534). No XRD patterns attributed to the crystalline phases of the promoters were observed. The Scherrer equation has provided information about the iron oxide particle size (**Table 1**). The addition of promoters Bi, Pb, and Sb (impregnated in second position) to the silica supported iron catalyst results in hematite crystallites with the sizes between 15-17 nm, which are comparable to the reference catalyst (17 nm). On the other side, the Sn promoted catalyst has the smallest crystallite size (11 nm). Consequently, with exception for Sn, these promoters seem have very slight effect on iron oxide dispersion.

We also carried out XRD measurements (**Figure 4b**) for non-promoted and promoted iron catalysts after FT reaction. The diffraction peaks around 2θ angle 44° for all catalysts are attributed to the iron carbide phase. In this case, the width of the iron carbide XRD peak clearly depends on the promoters. The apparent sizes of iron carbide nanoparticles calculated from XRD peak for promoted catalysts were between 4 and 6 nm, while for non-promoted

reference catalysts the iron particle size amounted to 12 nm. The results can be interpreted in terms of the better stability of the iron particles promoted with Sn, Sb, Bi and Pb versus sintering in the presence of carbon monoxide and reaction mixture. Recently, we found that promotion of iron catalysts with mobile promoters such as Bi and Pb results in less significant iron sintering and better catalyst stability [10,32]. In this paper, similar improvement of the stability of iron carbide nanoparticles towards sintering was also observed for the Sn- and Sb-promoted samples. **Figure S2, SI** shows very broad XRD peaks of iron carbide in the non-promoted Fe/SiO_2 catalyst activated in CO. These peaks are getting much narrower in the spent catalyst. Thus, iron sintering in the non-promoted Fe/SiO_2 catalyst does not occur during the activation in CO but in the course of FT reaction in the presence of syngas and reaction products

Figure 5 shows the H_2-TPR profiles measured for iron catalysts promoted with Sn, Sb, Pb, and Bi. As the promoted catalysts were prepared with a ratio of Fe:promoter 100:2, the hydrogen consumption amounts measured by TPR principally provide information about iron reduction. The amount of promoter was too small to noticeably contribute to the TPR peaks. The TPR profiles display several hydrogen consumption peaks, which are attributed to the multi-step iron reduction from Fe_2O_3 hematite to metallic iron.

$$Fe_2O_3 \rightarrow Fe_3O_4 \rightarrow FeO \rightarrow Fe$$

In agreement with previous reports [46–49], the first peak at 350-420 ^oC can be associated to the reduction of hematite (Fe_2O_3) to magnetite (Fe_3O_4), the second peak can be correlated to the reduction of magnetite (Fe_3O_4) to wüstite (FeO), whereas the third peak at 650-700^oC can be attributed to the reduction of wüstite (FeO) to metallic iron (Fe). The TPR peaks observed at T>1000°C can be related to barely reducible iron silicate species[50]. Interestingly, the promotion with mobile promoters only relatively slightly affects the positions of TPR peaks for iron catalysts. In general, all the promoted catalysts present a

better reducibility than the reference non-promoted iron catalyst. Fascinatingly, for Sb promoted catalysts the impregnation order has a significant effect on iron reducibility. A lower fraction of iron silicate species was observed in $SbFe/SiO_2$ compared to the $FeSb/SiO_2$. Introduction of Sb to silica before iron slows down interaction of iron with the support, which may result in iron silicates. It seems that the Sb impregnation after impregnation with iron favors iron reducibility and formation of iron metallic species. The characterization data suggest that the promotion of iron catalysts with Bi and Pb only slightly affects iron dispersion and iron reducibility. Iron dispersion is enhanced over the Sn-promoted catalyst, while iron reducibility is modified in the Sb- containing counterpart.

Further information about the genesis of active phases in non-promoted iron catalyst and catalysts promoted with tin and antimony was obtained using the *in-situ* magnetic method [37–39]. The Pb and Bi promoted silica supported iron catalysts were previously [33] characterized by the *in-situ* magnetic method. The dependence of magnetization on the temperature during exposure of non-promoted Fe/SiO_2 and tin- and antimony-promoted iron catalysts to CO is shown in **Figure 6**. The catalysts exhibit some low magnetization at room temperature. The magnetization of freshly calcined catalysts at room temperature can be due to the presence of ferromagnetic magnetite (Fe_3O_4) phase, which forms together with the hematite (Fe_2O_3) phase after the catalyst calcination. Heating of the catalysts in CO results in the increase in magnetization, which can be possibly due to the reduction of hematite into magnetite and formation of ferromagnetic iron carbide. Indeed, previously we showed [51] that carbidization of hematite proceeds via intermediate formation of magnetite. The magnetization drops at higher temperature for Fe/SiO_2 and $FeSn/SiO_2$ (**Figures 6a and b**), while the magnetization remains high for the catalyst promoted with antimony (**Figures 6c and d**). The decrease in the magnetization for the Fe/SiO_2 and $FeSn/SiO_2$ samples seems to be due to the formation of ferromagnetic phase with the Curie temperature lower than 250°C,

which can be Hägg iron carbide (T_{Curie}=205-256°C) or cementite (T_{Curie}=208°C)[12]. Higher magnetization observed for FeSb/SiO_2 and SbFe/SiO_2 samples seems to be due to the presence of the ferromagnetic phase with higher Curie temperature, possibly magnetite (T_{Curie}=585°C) [12].

The variation of magnetization during subsequent treatment of iron catalysts in syngas (H_2/CO=1) after their activation in CO is shown in **Figure 7**. All the samples display some magnetization at room temperature, which can be due to the presence of iron carbide or magnetite, which formed during the exposure to pure CO. Heating in syngas results in initial increase in the magnetization for Fe/SiO_2 and FeSn/SiO_2 samples (**Figures 7a and b**) due to further formation of iron carbide. The magnetization then drops at the temperatures higher than 250°C, which indicates the presence of iron carbides with Curie temperature lower than 250°C. Interestingly, for the FeSb/SiO_2 and SbFe/SiO_2 samples (**Figures 7c and d**), the magnetization drops during the temperature ramp in syngas without any initial increase. Magnetite has been formed in these samples during their pretreatment in CO. The decrease in magnetization during the subsequent exposure of FeSb/SiO_2 and SbFe/SiO_2 to syngas can be attributed to the carbidization of magnetite and formation of iron carbides. This suggests that the non-promoted iron catalyst and catalysts promoted with tin can be carbidized in CO, while the presence of syngas is required for carbidization of the catalysts promoted with antimony. It should be also noted that the non-promoted Fe/SiO_2 catalyst did not show any noticeable magnetization at 350°C. This indicates that almost all magnetite has been converted to iron carbides, while the catalysts promoted with tin or antimony exhibited residual magnetization even at high temperature. Thus, the presence of some amounts of residual magnetite in the Sn- and Sb-promoted catalysts is expected after activation in CO and syngas.

Information about the ferri- and ferromagnetic phases in the activated catalysts was further extracted from the thermomagnetic curves (**Figure S3, SI**). After the catalyst activation in CO and subsequently in syngas, the catalyst temperature was decreased from 350°C to ambient. All the catalysts showed an increase in magnetization during this temperature decrease. This suggests the presence of iron carbides with the Curie temperature between 200 and 250°C. Note that the magnetization increases in somewhat lower temperature for the non-promoted Fe/SiO_2 than for the promoted samples. This could be indicative of the cementite type carbide with lower Curie temperature (T_{Curie}=208°C) in Fe/SiO_2. In the promoted catalysts, the major iron carbide phase could be the Hagg Fe_5C_2 carbide.

3.3. Catalytic performance of the Sn-, Sb-, Bi and Pb-promoted catalysts.

The results of HTE catalytic tests have clearly indicated unusually high FT reaction rates of Sn-, Sb-, Bi and Pb-promoted iron catalysts compared to other counterparts (**Figure 1** and **Table 2**). All these four metals have relatively low melting points, i.e., Sn 232°C, Sb 630°C, Bi 271°C and Pb 328°C, compared to most of other metals. They possibly exist either in the liquid state or are highly mobile under FT reaction conditions. The reasons for the increase in FT reaction rate over the bismuth and lead promoted catalysts have been already discussed in our previous reports [10,11,32,33]. During the activation, bismuth and lead form the core-shell structures with iron species. The conducted kinetic and isotopic tracing experiments [33] indicated that the Bi and Pb promoters facilitated carbon monoxide dissociation by scavenging O atoms from the surface of iron carbide. Iron time yield (FTY) in the catalysts promoted with Bi, Pb, Sn and Sb increased 3-5 times (**Table 2**). The observed strong enhancement of FT reaction rate over the Bi and Pb-promoted iron catalysts obtained in this work is in agreement with previous reports[10,32,33].

Interestingly, in the present work, the Sb- and Sn-promoted catalysts also achieved remarkable reaction rate, which is much higher than for any other promoted iron catalysts (**Figure 1**). For the best of our knowledge, these are the first results relevant to the use of the Sn and Sb promoters for iron FT catalysts. The elements such as Sn and Sb are also (as Bi and Pb) located in groups IV and V of the Periodic Table and have similar properties. They exhibit several oxidation states. Their melting points are respectively situated at 232 and 630°C. High temperature FT synthesis proceeds in the temperature range between 300 and 350°C. This is higher that the Tamman temperature of all these metals (~0.5 of the melting point temperature measured in K). This suggests noticeable bulk mobility of Sb and Sn under the reaction conditions. Importantly, the carbon monoxide conversions and reaction rates for all non-promoted, Bi-, Pb-, Sn- and Sb-promoted catalysts observed either in the HTE or in laboratory fixed bed reactors are respectively rather similar (**Figure 1** and **Table 2**)

Catalyst deactivation remains one of the main challenges of FT synthesis. Deactivation results in the loss of catalytic activity with time on steam, low productivity and necessity to replace or to regenerate the catalysts. **Figure 8** shows variation of the carbon monoxide conversion with time on stream over the Sn-, Sb-, Bi- and Pb-promoted catalysts during the first 48 h of reaction. In agreement with previous reports[33], the reference non-promoted catalyst showed continuous decrease in the activity occurring until it reached a stable conversion of around 11 %. On the other hand, the iron catalysts promoted with Sn, Sb, Bi and Pb reached stable conversions after 10 h of reaction and they did not show appreciable deactivation during 48 h on stream. Better stability of iron catalyst with the Sb, Sb, Bi and Pb promoters can be therefore, attributed to less significant iron sintering. Indeed, XRD suggests (**Figure 4b)** highly dispersed iron carbides species in the spent promoted catalysts, while major iron sintering was observed during FT reaction in the non-promoted Fe/SiO_2. Indeed, formation of protective layer of quasi-liquid metal can slow down iron carbide sintering.

The catalytic tests show strong effect of the promotion with bismuth, tin, antimony and lead on the FT reaction rate (**Figure 2, Table 2**). High selectivity to light olefins is an extremely important reaction parameter and a major challenge of FT synthesis. In order to obtain more information about the effect of promotion with Bi, Sb, Sn and Pb on the reaction selectivities, the selectivity to different products was measured at a wide range of CO conversion. The selectivity conversion-curves (**Figure 9)** clearly emphasize the unique nature of bismuth and lead as the promoters, which at the same time, increase both overall reaction rate and light olefin selectivity. The data points for the light olefin selectivity plotted as a function of conversion over the catalysts promoted with bismuth and lead are clearly above the values observed for the Sn and Sb promoted counterparts and non-promoted iron catalysts (**Figure 9a**). The methane selectivity curves indicate lower values over the Bi- and Pb-promoted catalysts observed at the same CO conversion compared with the Sb-promoted and in particular Sn-promoted samples (**Figure 9b**). At the same time, the Bi and Pb –promoted catalysts exhibit lower selectivity to the C_2-C_4 paraffins compared with the Sb and Sb promoted counterparts (**Figure 9c**). The C_{5+} selectivity conversion curves measured for all four promoted catalysts do not indicate any major differences. (**Figure 9d**) They show general increase in the C_{5+} selectivity with the CO conversion. This suggests that the gain in the selectivity over the Bi and Pb promoted catalysts can be principally attributed to the decrease in the selectivity to methane and light paraffins. Indeed, the promotion of silica supported iron catalysts with Bi and Pb leads to a major increase in both FT reaction rate and light olefin selectivity, while tin and antimony when added to the silica supported iron catalysts have a major impact the FT reaction rate, but at the same time, they do not increase the light olefin selectivity.

4. Discussion

Mobile promoters for iron FT catalysts

Our work and previous reports show that the catalytic performance of iron catalysts can be significantly modified by addition of promoters. The promoters for iron FT catalyst can be either electronic or structural. The structural promoters do not affect the intrinsic activity of the active sites such as turnover frequency (TOF), but they modify the catalyst texture, enhance iron dispersion and improve the catalyst stability. Structural promoters of iron catalysts such as silica, alumina, or other oxides are essential to improve attrition resistance and stability especially for fluidized bed or slurry bed applications. However, structural promoters often hinder iron carbidization and decrease the activity due to the metal–support interactions and formation of iron support mixed compounds.

The electronic promoters interact directly with the active sites and affect the active sites intrinsic activity. The conventional electronic promoters for iron FT catalyst can be divided into three major groups: (i) alkali metals, (ii) transition metals and (iii) combined promotion with sodium and sulphur. Promotion of iron catalysts with alkali metals has been a subject of numerous publications [13,20,21,23,24,26,52]. Alkali ions added to iron catalysts can lead to the following effects on the catalytic performance: (1) an increase in the average molecular weight (chain length) of hydrocarbon products, i.e., decrease in production of methane and light gases, (2) an increase in olefin selectivity, (3) an increase in activity for the water gas shift (WGS) reaction, (4) an increase in carbon deposition and catalyst deactivation rate, and (5) an increase in reaction rate at low promoter concentrations, followed by decrease at higher concentrations.

The promotion with alkali metals increases olefin to paraffin ratio in the reaction products, while at the same time does not necessarily lead to higher selectivity to light olefins [26]. The promotion with alkali metals varies as a function of catalytic support [12]. In the presence of

oxide support, a part of iron and alkali species can form mixed oxide compounds, which decrease the amount of active iron carbide phase. Direct interaction of iron species and alkali can result in the electronic interaction with iron and modifies the intrinsic reaction rate and selectivity. It was suggested [24] that alkali ions could enhance carbon monoxide dissociation because of election-dative effect on the iron species coming from basic oxygen species.

The second group of promoters include transition metals and more particularly copper. Numerous studies have shown [8,28,53] that the addition of copper can result in an enhancement of the activity of Fe-based FT catalysts. The major copper function is to decrease the temperature required for the reduction of iron oxides, while the reports about the effect of copper on the selectivity are still controversial. Wachs et al. [54] and O'Brien et al. [55] observed that copper had no effect on the product selectivity. An increase in the average molecular weight of hydrocarbon products was reported over Cu-promoted iron catalysts by Bukur [7]. Coville [56] et al observed that the addition of Cu decreased the methane selectivity and had no significant effect on the catalytic activity. Mn-promoted Fe catalysts usually show higher light olefin selectivity compared to non-promoted Fe catalysts[57–60]. Molybdenum promoted Fe showed significant increase in the catalytic activity [61,62] an better olefin selectivity and enhanced stability[63]. Promotion with Cr enhanced the selectivity of precipitated Fe catalysts for longer chain hydrocarbon products [59,64].

The third type of promotion of iron catalysts has been recently proposed by de Jong [3,29,30] et al. The suggested method involved combined promotion of iron catalysts with sodium and sulphur. Higher C_2–C_4 olefin selectivity and less significant methane production were reported, while the overall activity is only slightly improved.

We uncovered a new type of promotion of iron catalysts with metals, which have low melting points such as tin, antimony, lead and bismuth. As discussed above, the presence of small amounts of these elements in iron catalysts results in a several fold increase in FT

reaction rates (**Figure 1**). The effect of these promoters on the FT reaction rate is one of the strongest ever observed in the literature [3,10]. The promotion with these elements has two particular features. First, these metals are highly mobile the under the conditions of high temperature FT synthesis. Their migration during catalyst activation and catalytic reaction has been clearly observed by TEM [32]. Second, these metals have several oxidation states. The mechanistic study [33] suggests that these elements can facilitate CO dissociation by scavenging oxygen from the surface of iron carbide by the promoters resulting in their re-oxidation.

Our results suggest that Bi, Pb, Sn and Sb can be considered as both electronic and structural promoters of iron FT catalysts. Though the presence of these metals has relatively small effect on iron dispersion in freshly prepared iron catalysts, however they stabilize iron carbide nanoparticles from sintering. **Figure 4** and **Figure S2, SI** show major sintering of iron carbide in the non-promoted Fe/SiO_2 catalyst after conducting FT reaction, while iron carbide remains highly dispersed in the promoted samples. The FT reaction rate remains stable over the promoted catalysts for at least 50 h (**Figure 8**). Previously we found that the promotion of Bi also resulted in better stability of cobalt catalysts in low temperature FT synthesis[43], where both carbon deposition and metal sintering were hindered.

While the iron dispersion is only slightly affected by the promotion with these elements, the increase in FT rate is principally attributed to the increase in the intrinsic activity. The observed increase in the FT reaction rate can be assigned to higher TOF (**Table 2**) due to the strong interaction of iron and promoters. The increase in TOF over the silica supported catalysts is consistent with our previous results [10], which showed 3-5 time increase in TOF on the promotion with Bi on iron catalysts supported over carbon nanotubes. This effect is probably due to the localization of the promoters in the close proximity to the iron carbide resulting in formation of core shell structures.

FT synthesis a complex multistage reaction. Hydrocarbon selectivity in FT synthesis is an interplay of several reaction steps and phenomena. This paper addresses general trends relevant to the selectivity variation with the conversion. The absolute selectivity values can be affected by the promoters and possibly by the support. Our results clearly suggest a significant increase in the selectivity to light olefins over the Bi and Pb-promoted samples, while the effect on the selectivity is much less significant over Sn- and Sb promoted counterparts. Different selectivity to light olefins observed over Bi-, Pb-promoted catalysts on the one hand, and over Sn and Sb counterparts on the other hand can be due to different hydrogenation activity. Indeed, the Sb and Sn promoted catalysts exhibit much higher methane selectivity and selectivities to light paraffins (**Figure 9**). At the same time, the selectivity to light olefins is not improved on the Sn and Sb promotion.

Conclusion

The catalyst tests conducted with silica supported iron catalysts promoted with 29 elements allowed identification general selectivity trends in FT synthesis. The selectivity was a function of promoters and reaction operating conditions. The light olefin selectivity close to 60% over iron catalysts is observed at low carbon monoxide conversion and then decreases with the conversion. The methane and light paraffin selectivities follow similar trend. The selectivity to carbon dioxide increases with carbon monoxide conversion and reaches the stoichiometric values of 50% at the carbon monoxide conversion higher than 30%. The selectivity to the C_{5+} long chain hydrocarbons increases with carbon monoxide conversion. In order to obtain high selectivity to light olefins, the selectivity to light paraffins and long chain C_{5+} hydrocarbons should be minimized in particular, at higher CO conversion.

Promotion of iron catalysts with metals with low melting points such as Bi, Pb, Sn and Sb resulted in a major increase (several fold) in FT reaction rate. This promotion also results in

higher intrinsic activity of surface sites. Two types of the promotion were observed. The promotion with Sn and Sn results only in the enhancement of the FT reaction rate, while the light olefin selectivity is not much affected. The promotion with Bi and Pb leads to the increase in both the FT reaction rate and selectivity to light olefins.

Acknowledgements

The authors acknowledge financial support from European Union (Interreg V project PSYCHE). The REALCAT platform is benefiting from a Governmental subvention administrated by the French National Research Agency (ANR) within the frame of the 'Future Investments' program (PIA), with contractual reference 'ANR-11-EQPX-0037'.

References

[1] E. van Steen, M. Claeys, Fischer-Tropsch Catalysts for the Biomass-to-Liquid (BTL)-Process, Chem. Eng. Technol. 31 (2008) 655–666. https://doi.org/10.1002/ceat.200800067.

[2] Q. Zhang, J. Kang, Y. Wang, Development of Novel Catalysts for Fischer-Tropsch Synthesis: Tuning the Product Selectivity, ChemCatChem. 2 (2010) 1030–1058. https://doi.org/10.1002/cctc.201000071.

[3] H.M. Torres Galvis, J.H. Bitter, C.B. Khare, M. Ruitenbeek, A.I. Dugulan, K.P. de Jong, Supported Iron Nanoparticles as Catalysts for Sustainable Production of Lower Olefins, Science (80-.). 335 (2012) 835–838. https://doi.org/10.1126/science.1215614.

[4] M.E. Dry, The Fischer–Tropsch process: 1950–2000, Catal. Today. 71 (2002) 227–241. https://doi.org/10.1016/S0920-5861(01)00453-9.

[5] H.M. Torres Galvis, K.P. de Jong, Catalysts for Production of Lower Olefins from Synthesis Gas: A Review, ACS Catal. 3 (2013) 2130–2149. https://doi.org/10.1021/cs4003436.

[6] E. de Smit, B.M. Weckhuysen, The renaissance of iron-based Fischer–Tropsch synthesis: on the multifaceted catalyst deactivation behaviour, Chem. Soc. Rev. 37 (2008) 2758. https://doi.org/10.1039/b805427d.

[7] D.B. Bukur, D. Mukesh, S.A. Patel, Promoter effects on precipitated iron catalysts for Fischer-Tropsch synthesis, Ind. Eng. Chem. Res. 29 (1990) 194–204. https://doi.org/10.1021/ie00098a008.

[8] N. Lohitharn, J.G. Goodwin Jr., E. Lotero, Fe-based Fischer–Tropsch synthesis catalysts containing carbide-forming transition metal promoters, J. Catal. 255 (2008)

104–113. https://doi.org/10.1016/j.jcat.2008.01.026.

[9] W. Chen, Z. Fan, X. Pan, X. Bao, Effect of Confinement in Carbon Nanotubes on the Activity of Fischer−Tropsch Iron Catalyst, J. Am. Chem. Soc. 130 (2008) 9414–9419. https://doi.org/10.1021/ja8008192.

[10] B. Gu, S. He, D.V.D. V. Peron, D.R.D.R. Strossi Pedrolo, S. Moldovan, M.C.M.C. Ribeiro, B. Lobato, P.A.P.A. Chernavskii, V.V.V. V. Ordomsky, A.Y.A.Y. Khodakov, Synergy of nanoconfinement and promotion in the design of efficient supported iron catalysts for direct olefin synthesis from syngas, J. Catal. 376 (2019) 1–16. https://doi.org/10.1016/j.jcat.2019.06.035.

[11] B. Gu, C. Zhou, S. He, S. Moldovan, P.A.P.A. Chernavskii, V.V.V. V. Ordomsky, A.Y.A.Y. Khodakov, Size and promoter effects on iron nanoparticles confined in carbon nanotubes and their catalytic performance in light olefin synthesis from syngas, Catal. Today. (2019). https://doi.org/10.1016/j.cattod.2019.05.054.

[12] K. Cheng, V.V. Ordomsky, M. Virginie, B. Legras, P.A. Chernavskii, V.O. Kazak, C. Cordier, S. Paul, Y. Wang, A.Y. Khodakov, Support effects in high temperature Fischer-Tropsch synthesis on iron catalysts, Appl. Catal. A Gen. 488 (2014). https://doi.org/10.1016/j.apcata.2014.09.033.

[13] R.A. Dictor, A.T. Bell, Fischer-Tropsch synthesis over reduced and unreduced iron oxide catalysts, J. Catal. 97 (1986) 121–136. https://doi.org/10.1016/0021-9517(86)90043-6.

[14] S. Li, G.D. Meitzner, E. Iglesia, Structure and Site Evolution of Iron Oxide Catalyst Precursors during the Fischer−Tropsch Synthesis, J. Phys. Chem. B. 105 (2001) 5743–5750. https://doi.org/10.1021/jp010288u.

[15] V.V. Ordomsky, B. Legras, K. Cheng, S. Paul, A.Y. Khodakov, The role of carbon atoms of supported iron carbides in Fischer-Tropsch synthesis, Catal. Sci. Technol. 5

(2015) 1433–1437. https://doi.org/10.1039/c4cy01631a.

[16] T. Herranz, S. Rojas, F. Perezalonso, M. Ojeda, P. Terreros, J. Fierro, Genesis of iron carbides and their role in the synthesis of hydrocarbons from synthesis gas, J. Catal. 243 (2006) 199–211. https://doi.org/10.1016/j.jcat.2006.07.012.

[17] C. Yang, H. Zhao, Y. Hou, D. Ma, Fe 5 C 2 Nanoparticles: A Facile Bromide-Induced Synthesis and as an Active Phase for Fischer–Tropsch Synthesis, J. Am. Chem. Soc. 134 (2012) 15814–15821. https://doi.org/10.1021/ja305048p.

[18] B.H. Davis, Fischer−Tropsch Synthesis: Comparison of Performances of Iron and Cobalt Catalysts, Ind. Eng. Chem. Res. 46 (2007) 8938–8945. https://doi.org/10.1021/ie0712434.

[19] B.H. Davis, Fischer–Tropsch Synthesis: Reaction mechanisms for iron catalysts, Catal. Today. 141 (2009) 25–33. https://doi.org/10.1016/j.cattod.2008.03.005.

[20] M.C. Ribeiro, G. Jacobs, B.H. Davis, D.C. Cronauer, A.J. Kropf, C.L. Marshall, Fischer−Tropsch Synthesis: An In-Situ TPR-EXAFS/XANES Investigation of the Influence of Group I Alkali Promoters on the Local Atomic and Electronic Structure of Carburized Iron/Silica Catalysts, J. Phys. Chem. C. 114 (2010) 7895–7903. https://doi.org/10.1021/jp911856q.

[21] J. Li, X. Cheng, C. Zhang, J. Wang, W. Dong, Y. Yang, Y. Li, Alkalis in iron-based Fischer-Tropsch synthesis catalysts: distribution, migration and promotion, J. Chem. Technol. Biotechnol. 92 (2017) 1472–1480. https://doi.org/10.1002/jctb.5152.

[22] N. Lohitharn, J.G. Goodwin, Effect of K promotion of Fe and FeMn Fischer–Tropsch synthesis catalysts: Analysis at the site level using SSITKA, J. Catal. 260 (2008) 7–16. https://doi.org/10.1016/j.jcat.2008.08.011.

[23] H. Arakawa, A.T. Bell, Effects of potassium promotion on the activity and selectivity of iron Fischer-Tropsch catalysts, Ind. Eng. Chem. Process Des. Dev. 22 (1983) 97–

103. https://doi.org/10.1021/i200020a017.

[24] W. Ngantsoue-Hoc, Y. Zhang, R.J. O'Brien, M. Luo, B.H. Davis, Fischer–Tropsch synthesis: activity and selectivity for Group I alkali promoted iron-based catalysts, Appl. Catal. A Gen. 236 (2002) 77–89. https://doi.org/10.1016/S0926-860X(02)00278-8.

[25] P.A. Chernavskii, V.O. Kazak, G.V. Pankina, Y.D. Perfiliev, T. Li, M. Virginie, A.Y. Khodakov, Influence of copper and potassium on the structure and carbidisation of supported iron catalysts for Fischer-Tropsch synthesis, Catal. Sci. Technol. 7 (2017) 2325–2334. https://doi.org/10.1039/c6cy02676a.

[26] K. Cheng, V.V. Ordomsky, B. Legras, M. Virginie, S. Paul, Y. Wang, A.Y. Khodakov, Sodium-promoted iron catalysts prepared on different supports for high temperature Fischer-Tropsch synthesis, Appl. Catal. A Gen. 502 (2015). https://doi.org/10.1016/j.apcata.2015.06.010.

[27] V.R.R. Pendyala, G. Jacobs, M.K. Gnanamani, Y. Hu, A. MacLennan, B.H. Davis, Selectivity control of Cu promoted iron-based Fischer-Tropsch catalyst by tuning the oxidation state of Cu to mimic K, Appl. Catal. A Gen. 495 (2015) 45–53. https://doi.org/10.1016/j.apcata.2015.01.027.

[28] D. Peña, L. Jensen, A. Cognigni, R. Myrstad, T. Neumayer, W. van Beek, M. Rønning, The Effect of Copper Loading on Iron Carbide Formation and Surface Species in Iron-Based Fischer-Tropsch Synthesis Catalysts, ChemCatChem. 10 (2018) 1300–1312. https://doi.org/10.1002/cctc.201701673.

[29] H.M. Torres Galvis, A.C.J. Koeken, J.H. Bitter, T. Davidian, M. Ruitenbeek, A.I. Dugulan, K.P. de Jong, Effects of sodium and sulfur on catalytic performance of supported iron catalysts for the Fischer–Tropsch synthesis of lower olefins, J. Catal. 303 (2013) 22–30. https://doi.org/10.1016/j.jcat.2013.03.010.

[30] J. Xie, J. Yang, A.I. Dugulan, A. Holmen, D. Chen, K.P. de Jong, M.J. Louwerse, Size and Promoter Effects in Supported Iron Fischer–Tropsch Catalysts: Insights from Experiment and Theory, ACS Catal. 6 (2016) 3147–3157. https://doi.org/10.1021/acscatal.6b00131.

[31] G.F. Botes, T.C. Bromfield, R.L.J. Coetzer, R. Crous, P. Gibson, A.C. Ferreira, Development of a chemical selective iron Fischer Tropsch catalyst, Catal. Today. 275 (2016) 40–48. https://doi.org/10.1016/j.cattod.2015.11.044.

[32] B. Gu, V.V. Ordomsky, M. Bahri, O. Ersen, P.A. Chernavskii, D. Filimonov, A.Y. Khodakov, Effects of the promotion with bismuth and lead on direct synthesis of light olefins from syngas over carbon nanotube supported iron catalysts, Appl. Catal. B Environ. 234 (2018) 153–166. https://doi.org/10.1016/j.apcatb.2018.04.025.

[33] V.V. Ordomsky, Y. Luo, B. Gu, A. Carvalho, P.A. Chernavskii, K. Cheng, A.Y. Khodakov, Soldering of iron catalysts for direct synthesis of light olefins from syngas under mild reaction conditions, ACS Catal. 7 (2017) 6445–6452. https://doi.org/10.1021/acscatal.7b01307.

[34] C.L. Allen, D.C. Leitch, M.S. Anson, M.A. Zajac, The power and accessibility of high-throughput methods for catalysis research, Nat. Catal. 2 (2019) 2–4. https://doi.org/10.1038/s41929-018-0220-4.

[35] E.S. Isbrandt, R.J. Sullivan, S.G. Newman, High Throughput Strategies for the Discovery and Optimization of Catalytic Reactions, Angew. Chemie Int. Ed. 58 (2019) 7180–7191. https://doi.org/10.1002/anie.201812534.

[36] W.F. Maier, Early Years of High-Throughput Experimentation and Combinatorial Approaches in Catalysis and Materials Science, ACS Comb. Sci. 21 (2019) 437–444. https://doi.org/10.1021/acscombsci.8b00189.

[37] P.A. Chernavskii, B.S. Lunin, R.A. Zakharyan, G. V. Pankina, N.S. Perov,

Experimental setup for investigating topochemical transformations of ferromagnetic nanoparticles, Instruments Exp. Tech. 57 (2014) 78–81. https://doi.org/10.1134/S0020441214010035.

[38] P.A. Chernavskii, J.-A. Dalmon, N.S. Perov, A.Y. Khodakov, Magnetic characterization of Fischer-Tropsch catalysts, Oil Gas Sci. Technol. 64 (2009) 25–48. https://doi.org/10.2516/ogst/2008050.

[39] P.A. Chernavskii, A.Y. Khodakov, G.V. Pankina, J.-S. Girardon, E. Quinet, In situ characterization of the genesis of cobalt metal particles in silica-supported Fischer-Tropsch catalysts using Foner magnetic method, Appl. Catal. A Gen. 306 (2006) 108–119. https://doi.org/10.1016/j.apcata.2006.03.033.

[40] K. Cheng, M. Virginie, V.V. Ordomsky, C. Cordier, P.A. Chernavskii, M.I. Ivantsov, S. Paul, Y. Wang, A.Y. Khodakov, Pore size effects in higherature Fischer-Tropsch synthesis over supported iron catalysts, J. Catal. 328 (2015). https://doi.org/10.1016/j.jcat.2014.12.007.

[41] V.K. Jones, L.R. Neubauer, C.H. Bartholomew, Effects of crystallite size and support on the carbon monoxide hydrogenation activity/selectivity properties of iron/carbon, J. Phys. Chem. 90 (1986) 4832–4839. https://doi.org/10.1021/j100411a023.

[42] H.M. Torres Galvis, J.H. Bitter, T. Davidian, M. Ruitenbeek, A.I. Dugulan, K.P. de Jong, Iron Particle Size Effects for Direct Production of Lower Olefins from Synthesis Gas, J. Am. Chem. Soc. 134 (2012) 16207–16215. https://doi.org/10.1021/ja304958u.

[43] H. Schulz, Selforganization in Fischer–Tropsch synthesis with iron- and cobalt catalysts, Catal. Today. 228 (2014) 113–122. https://doi.org/10.1016/j.cattod.2013.11.060.

[44] M. Ojeda, R. Nabar, A.U. Nilekar, A. Ishikawa, M. Mavrikakis, E. Iglesia, CO activation pathways and the mechanism of Fischer–Tropsch synthesis, J. Catal. 272

(2010) 287–297. https://doi.org/10.1016/j.jcat.2010.04.012.

[45] T.H. Pham, X. Duan, G. Qian, X. Zhou, D. Chen, CO Activation Pathways of Fischer–Tropsch Synthesis on χ-Fe 5 C 2 (510): Direct versus Hydrogen-Assisted CO Dissociation, J. Phys. Chem. C. 118 (2014) 10170–10176. https://doi.org/10.1021/jp502225r.

[46] G. Yu, B. Sun, Y. Pei, S. Xie, S. Yan, M. Qiao, K. Fan, X. Zhang, B. Zong, Fe x O y @C Spheres as an Excellent Catalyst for Fischer−Tropsch Synthesis, J. Am. Chem. Soc. 132 (2010) 935–937. https://doi.org/10.1021/ja906370b.

[47] V. Subramanian, V.V. Ordomsky, B. Legras, K. Cheng, C. Cordier, P.A. Chernavskii, A.Y. Khodakov, Design of iron catalysts supported on carbon-silica composites with enhanced catalytic performance in high-temperature Fischer-Tropsch synthesis, Catal. Sci. Technol. 6 (2016) 4953–4961. https://doi.org/10.1039/c6cy00060f.

[48] M.D. Romero, A. de Lucas, J.A. Calles, A. Rodríguez, Bifunctional catalyst NiHZSM-5: effects of the nickel incorporation method, Appl. Catal. A Gen. 146 (1996) 425–441. https://doi.org/https://doi.org/10.1016/S0926-860X(96)00146-9.

[49] K. Mai, T. Elder, L.H. Groom, J.J. Spivey, Fe-based Fischer Tropsch synthesis of biomass-derived syngas: Effect of synthesis method, Catal. Commun. 65 (2015) 76–80. https://doi.org/10.1016/j.catcom.2015.02.027.

[50] K. Yogo, S. Tanaka, T. Ono, T. Mikami, E. Kikuchi, Characterization of Fe-silicates and their catalytic properties for the selective reduction of nitric oxide by hydrocarbons, Microporous Mater. 3 (1994) 39–46. https://doi.org/10.1016/0927-6513(94)00004-2.

[51] P.A. Chernavskii, V.O. Kazak, G.V. Pankina, V.V. Ordomsky, A.Y. Khodakov, Mechanistic aspects of the activation of silica-supported iron catalysts for Fischer-Tropsch synthesis in carbon monoxide and syngas, ChemCatChem. 8 (2016) 390–395.

https://doi.org/10.1002/cctc.201500811.

[52] T.J. Donnelly, C.N. Satterfield, Product distributions of the Fischer-Tropsch synthesis on precipitated iron catalysts, Appl. Catal. 52 (1989) 93–114. https://doi.org/10.1016/S0166-9834(00)83375-8.

[53] P.A. Chernavskii, V.O. Kazak, G. V. Pankina, Y.D. Perfiliev, T. Li, M. Virginie, A.Y. Khodakov, Influence of copper and potassium on the structure and carbidisation of supported iron catalysts for Fischer–Tropsch synthesis, Catal. Sci. Technol. 7 (2017) 2325–2334. https://doi.org/10.1039/C6CY02676A.

[54] I. E. Wachs, D. J. Dwyer, E. Iglesia, Characterization of Fe, Fe-Cu, And Fe-Ag fischer-tropsch catalysts, Appl. Catal. 12 (1984) 201–217. https://doi.org/10.1016/S0166-9834(00)80291-2.

[55] R.J. O'Brien, B.H. Davis, Impact of Copper on an Alkali Promoted Iron Fischer–Tropsch Catalyst, Catal. Letters. 94 (2004) 1–6. https://doi.org/10.1023/B:CATL.0000019322.69160.ef.

[56] H. Xiong, M. Moyo, M.A.M. Motchelaho, L.L. Jewell, N.J. Coville, Fischer–Tropsch synthesis over model iron catalysts supported on carbon spheres: The effect of iron precursor, support pretreatment, catalyst preparation method and promoters, Appl. Catal. A Gen. 388 (2010) 168–178. https://doi.org/10.1016/j.apcata.2010.08.039.

[57] J. Abbott, N.J. Clark, B.G. Baker, Effects of sodium, aluminium and manganese on the fischer-tropsch synthesis over alumina-supported iron catalysts, Appl. Catal. 26 (1986) 141–153. https://doi.org/10.1016/S0166-9834(00)82547-6.

[58] J.-D. Xu, K.-T. Zhu, X.-F. Weng, W.-Z. Weng, C.-J. Huang, H.-L. Wan, Carbon nanotube-supported Fe–Mn nanoparticles: A model catalyst for direct conversion of syngas to lower olefins, Catal. Today. 215 (2013) 86–94. https://doi.org/10.1016/j.cattod.2013.04.018.

[59] H. Wang, Y. Yang, J. Xu, H. Wang, M. Ding, Y. Li, Study of bimetallic interactions and promoter effects of FeZn, FeMn and FeCr Fischer–Tropsch synthesis catalysts, J. Mol. Catal. A Chem. 326 (2010) 29–40. https://doi.org/10.1016/j.molcata.2010.04.009.

[60] T. Herranz, S. Rojas, M. Ojeda, F.J. Pérez-Alonso, P. Terreros, K. Pirota, J.L.G. Fierro, Synthesis, Structural Features, and Reactivity of Fe−Mn Mixed Oxides Prepared by Microemulsion, Chem. Mater. 18 (2006) 2364–2375. https://doi.org/10.1021/cm052568i.

[61] S. Qin, C. Zhang, J. Xu, B. Wu, H. Xiang, Y. Li, Effect of Mo addition on precipitated Fe catalysts for Fischer–Tropsch synthesis, J. Mol. Catal. A Chem. 304 (2009) 128–134. https://doi.org/10.1016/j.molcata.2009.02.001.

[62] A. Alayat, E. Echeverria, D.N. Mcllroy, A.G. McDonald, Enhancement of the catalytic performance of silica nanosprings (NS)-supported iron catalyst with copper, molybdenum, cobalt and ruthenium promoters for Fischer-Tropsch synthesis, Fuel Process. Technol. 177 (2018) 89–100. https://doi.org/10.1016/j.fuproc.2018.04.020.

[63] R.M. Malek Abbaslou, J. Soltan, A.K. Dalai, Iron catalyst supported on carbon nanotubes for Fischer–Tropsch synthesis: Effects of Mo promotion, Fuel. 90 (2011) 1139–1144. https://doi.org/10.1016/j.fuel.2010.10.044.

[64] D.J. Duvenhage, N.J. Coville, Effect of K, Mn and Cr on the Fischer–Tropsch Activity of Fe:Co/TiO2 Catalysts, Catal. Letters. 104 (2005) 129–133. https://doi.org/10.1007/s10562-005-7941-0.

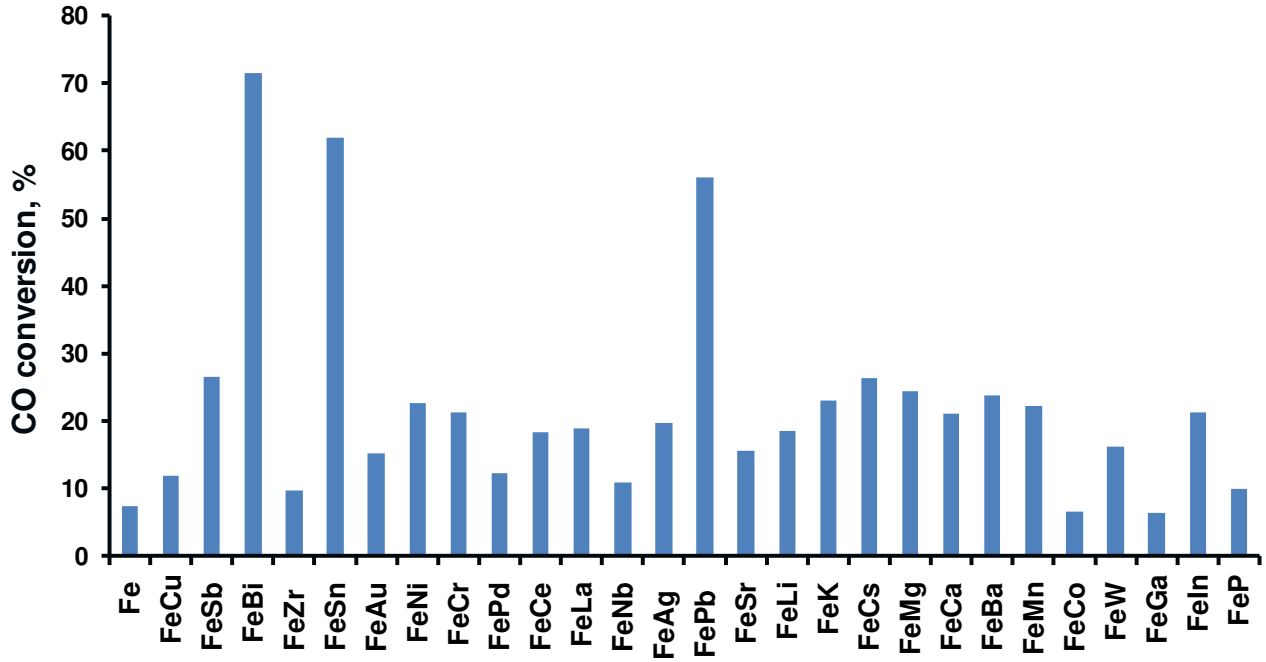

Figure 1. Carbon monoxide conversion measured over the promoted silica supported iron catalysts at iso-WHSV: T=350ºC, H_2/CO=1, p=10 bar, WHSV=3.4 L/g·h.

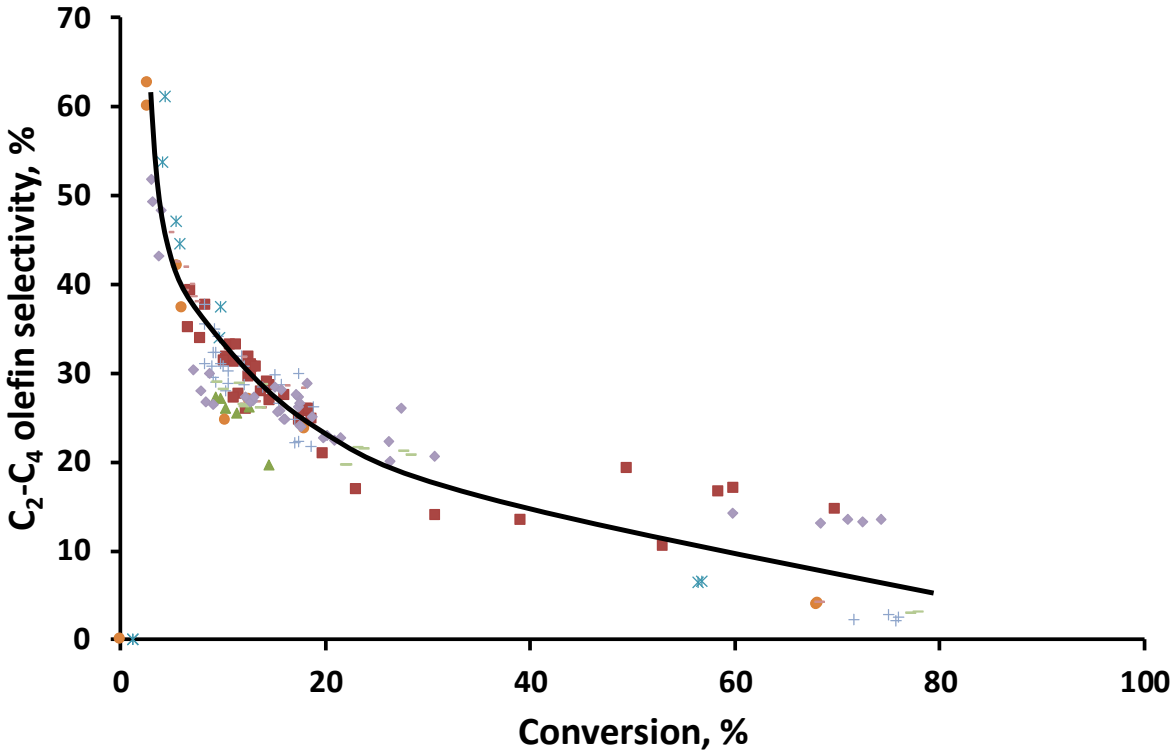

Figure 2. Light olefin selectivity versus carbon monoxide conversion. Promoted Fe/SiO_2, catalysts. Fe/P=100:2, H_2/CO=1, WHSV=2.25-675 L/ g h, p=10 bar

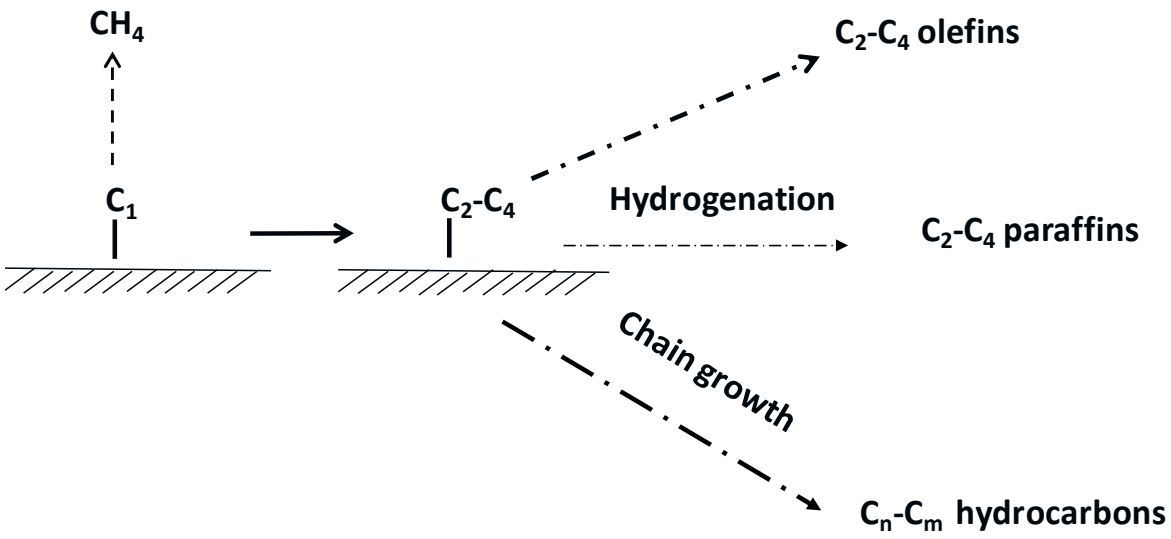

Figure 3. Surface polymerization paths in high temperature FT synthesis over iron catalysts

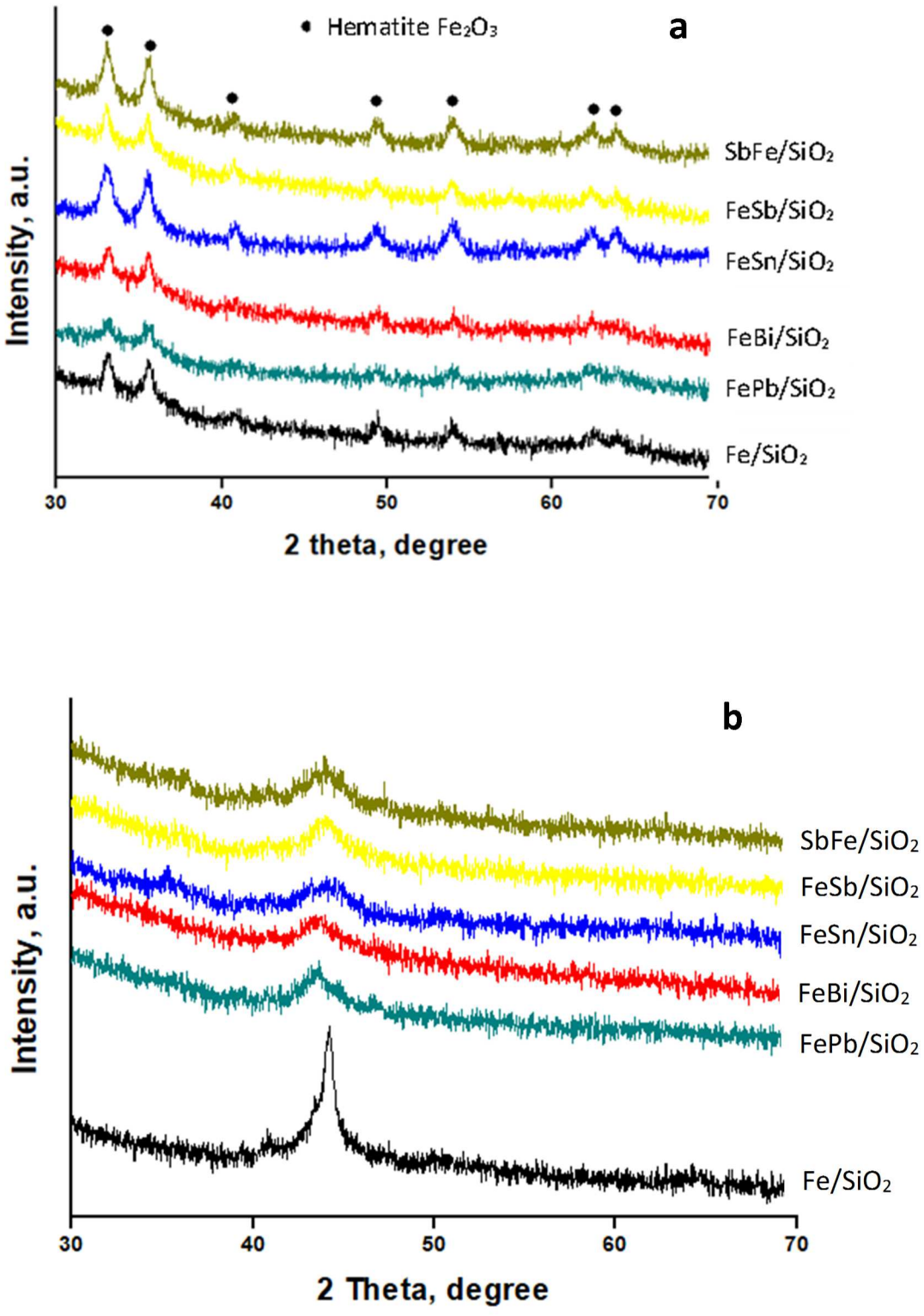

Figure 4. XRD patterns of the catalysts after calcination (a) and after FT reaction (b).

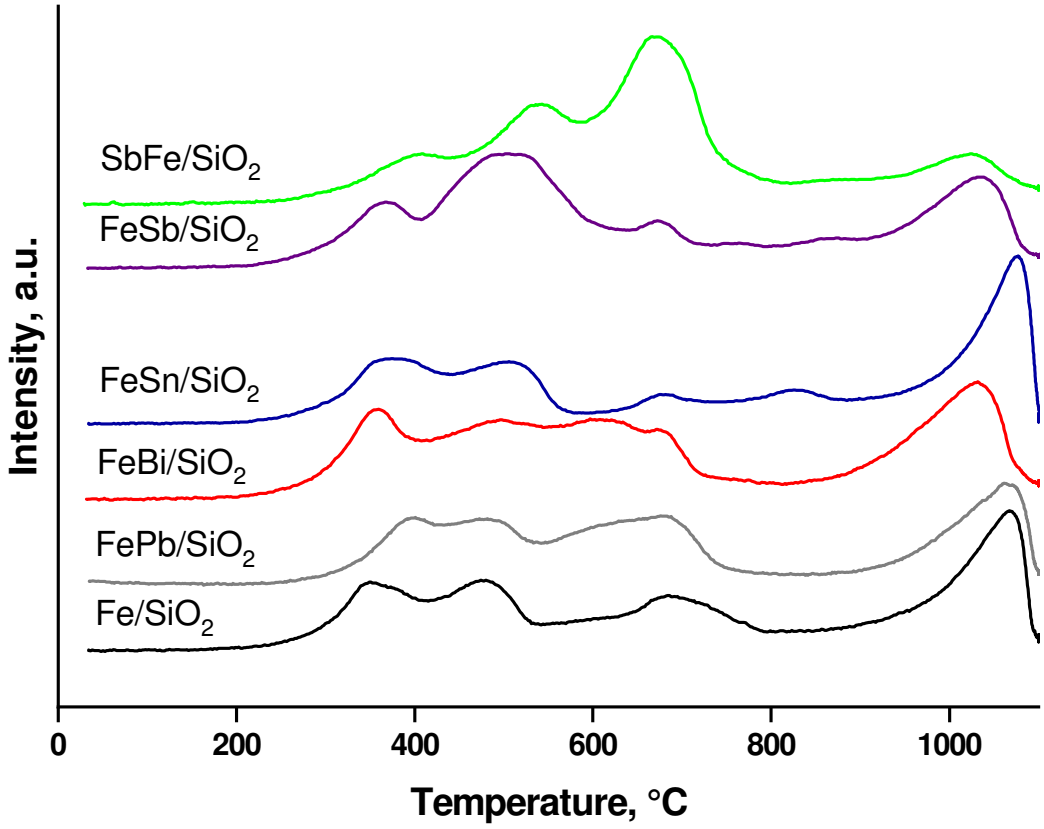

Figure 5. H_2-TPR profiles of reference and promoted catalysts with Sn, Sb, Bi and Pb.

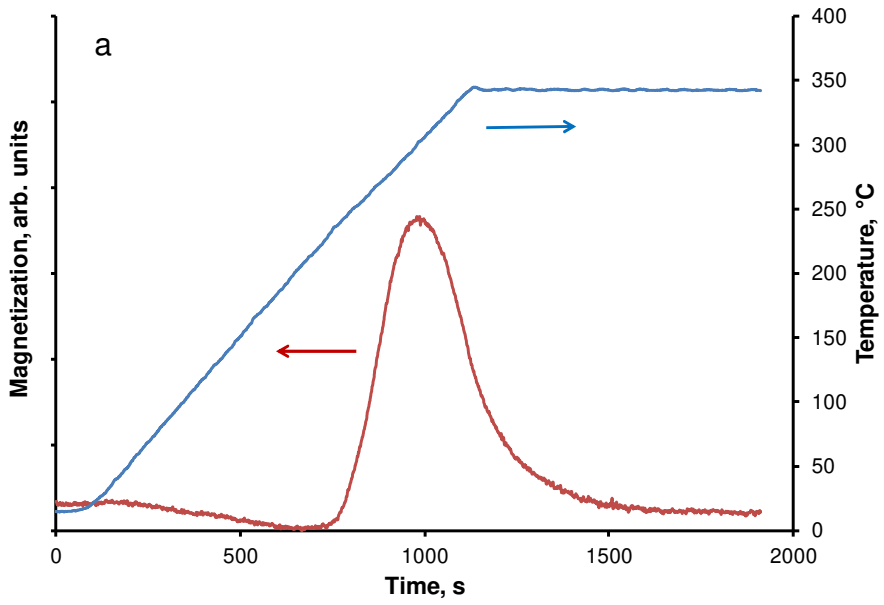
a
Magnetization, arb. units
Temperature, °C
Time, s
0
500
1000
1500
2000
0
50
100
150
200
250
300
350
400

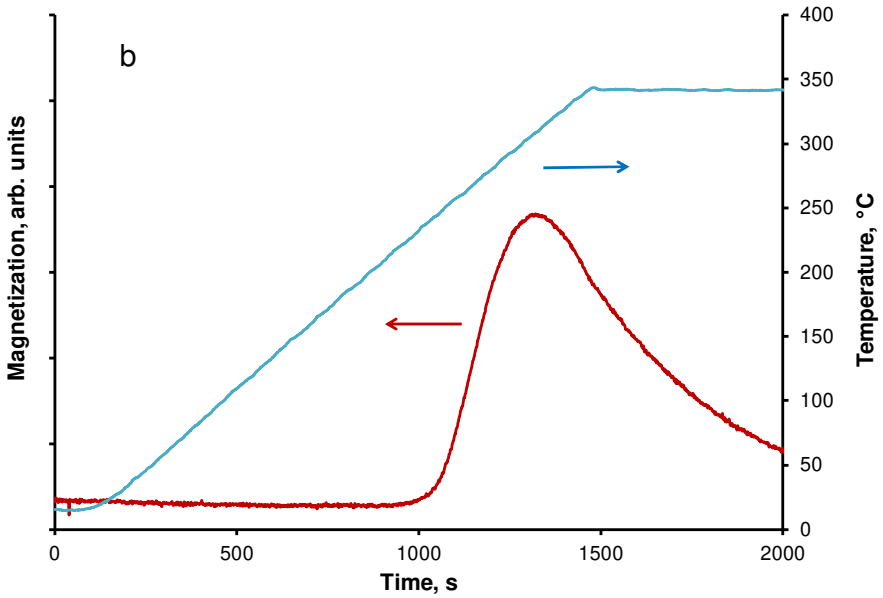
b
Magnetization, arb. units
Temperature, °C
Time, s
0
500
1000
1500
2000
0
50
100
150
200
250
300
350
400

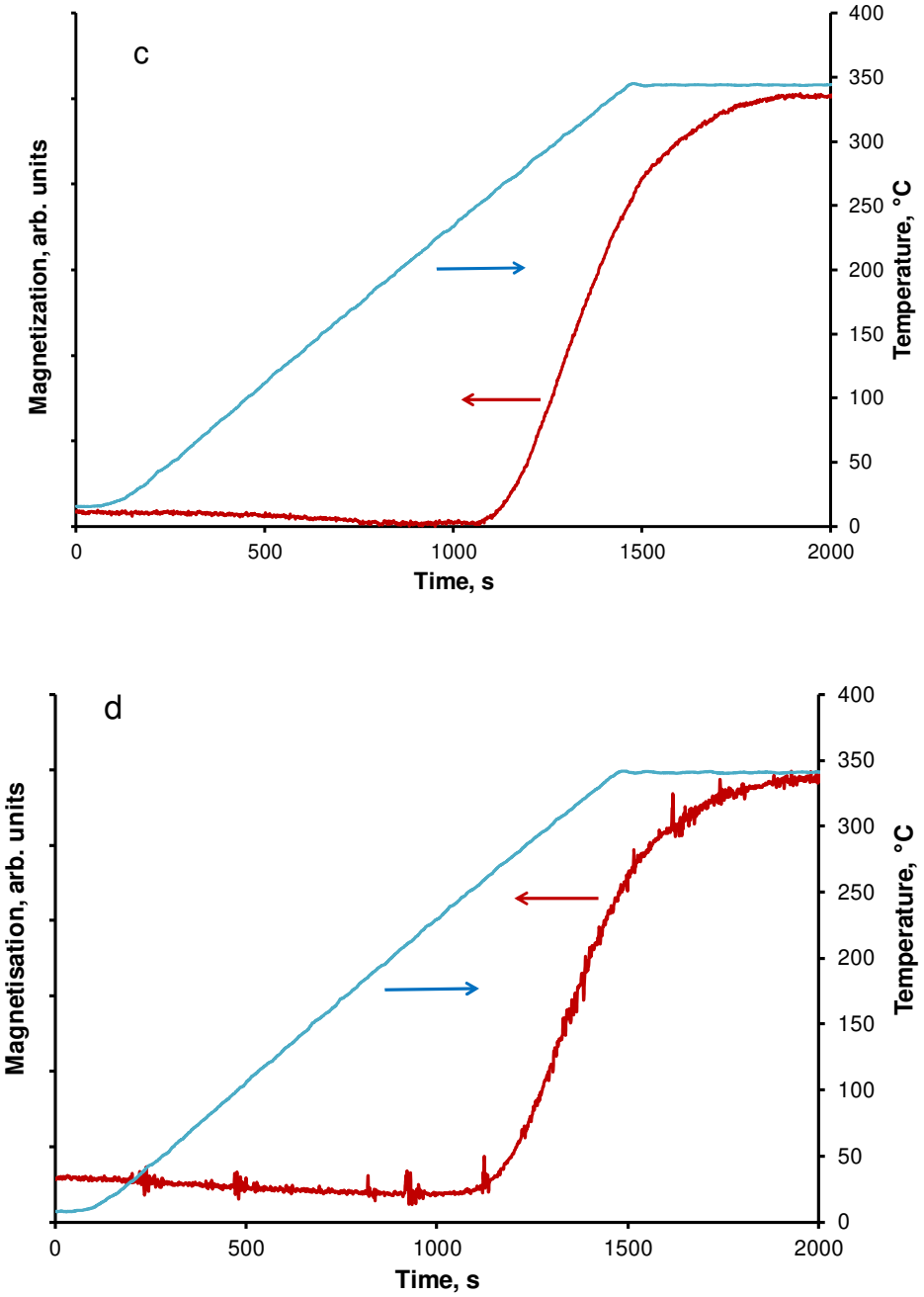

Figure 6. Variation of magnetization during exposure of silica supported iron catalysts to CO as a function of temperature (a- Fe/SiO_2, b- $FeSn/SiO_2$; c- $FeSb/SiO_2$, d- $SbFe/SiO_2$).

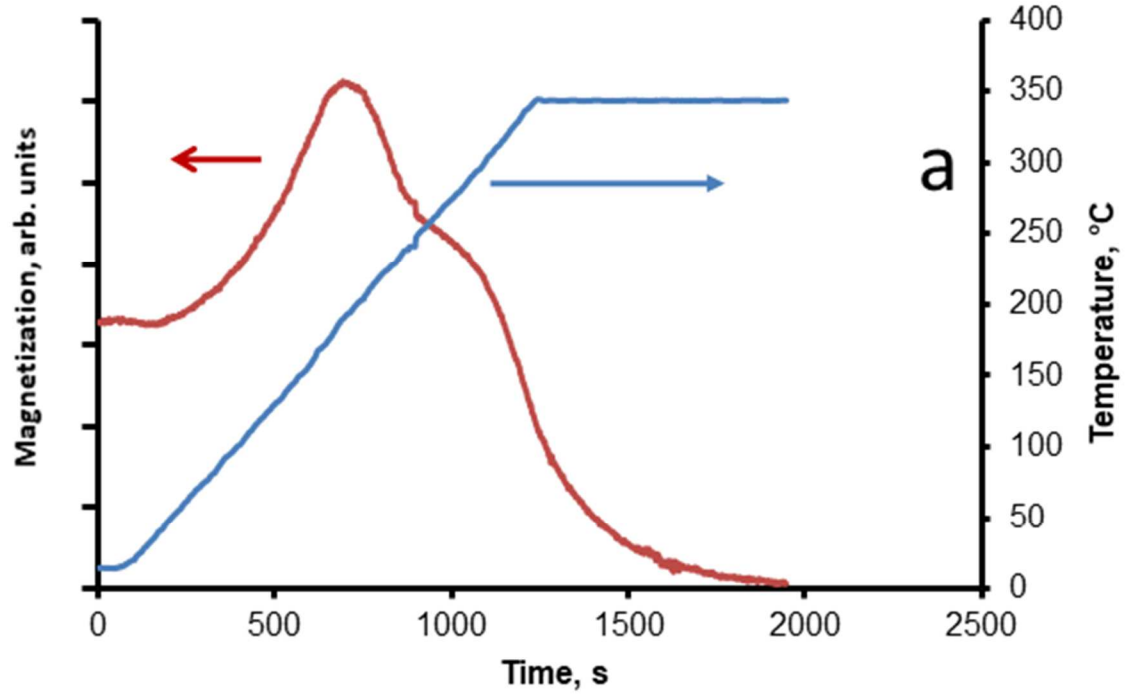
Magnetization, arb. units
Temperature, °C
Time, s
a
0
500
1000
1500
2000
2500
0
50
100
150
200
250
300
350
400

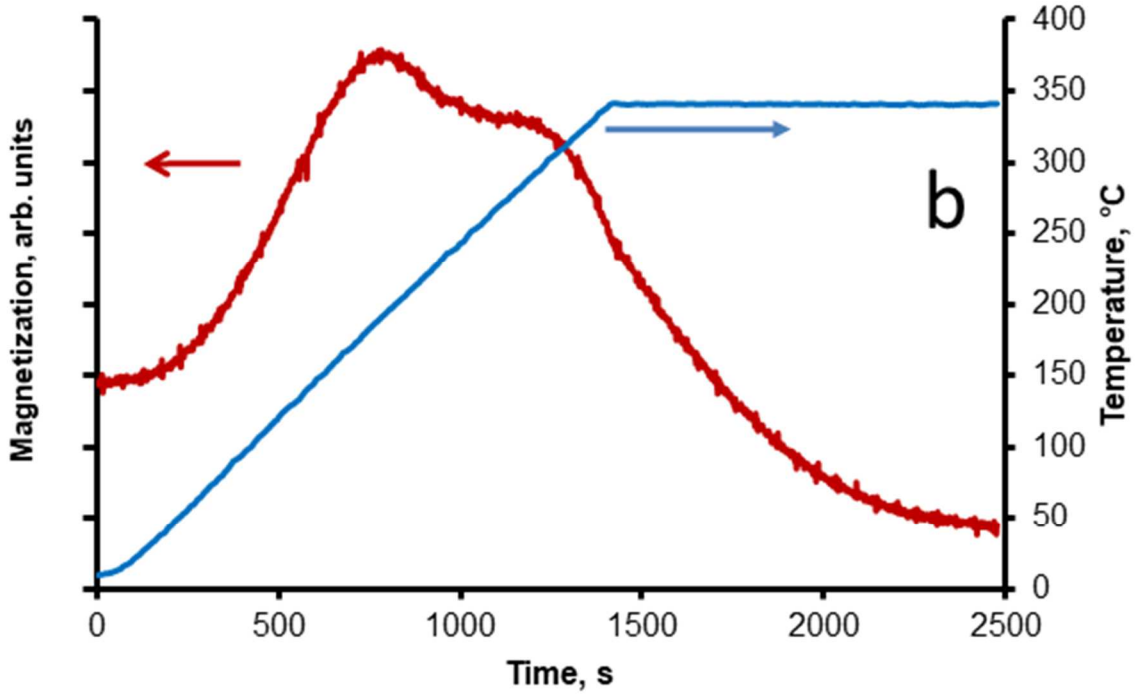
Magnetization, arb. units
Temperature, °C
Time, s
b
0
500
1000
1500
2000
2500
0
50
100
150
200
250
300
350
400

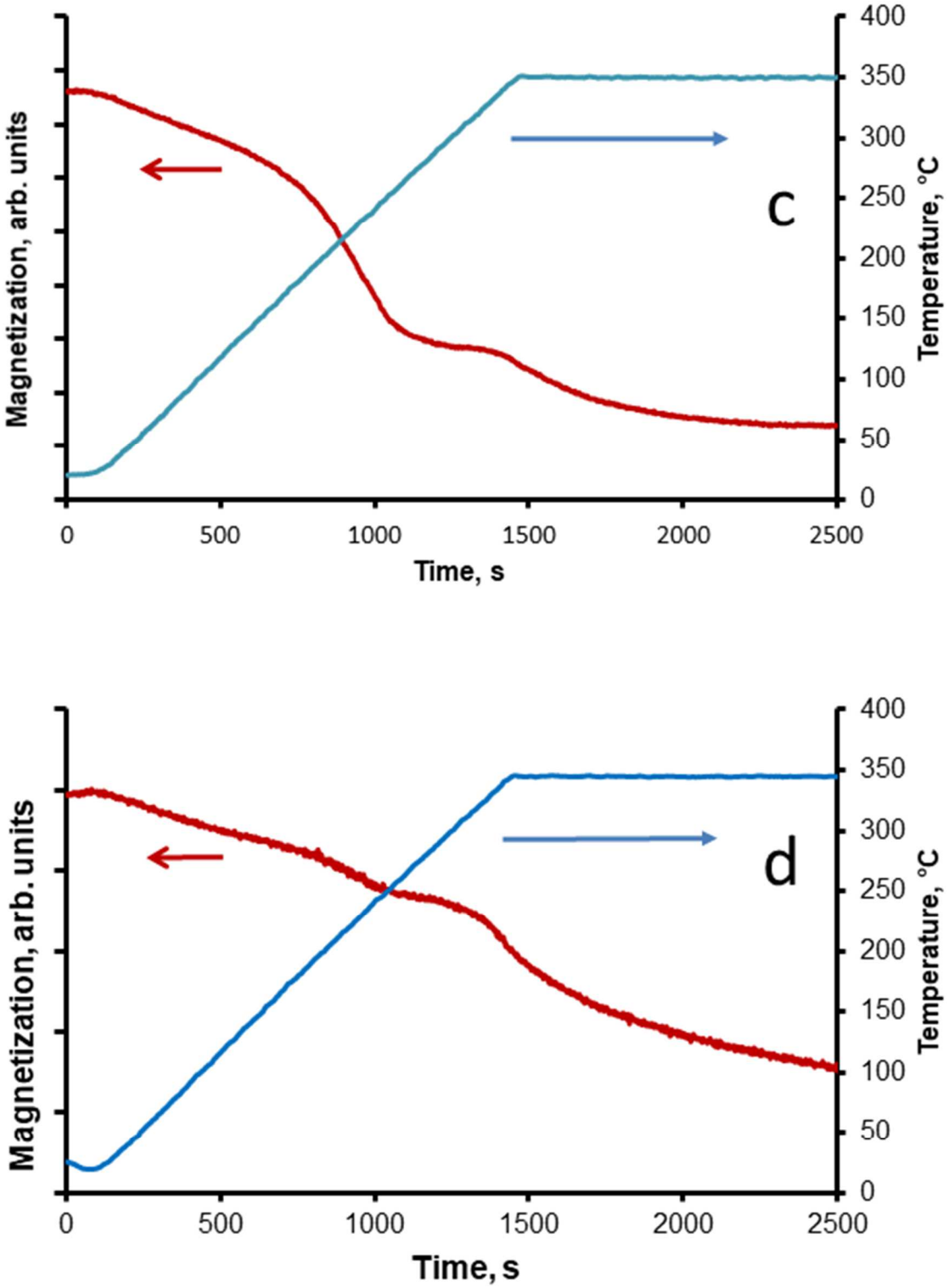

Figure 7. Variation of magnetization during exposure of silica supported iron catalysts activated in pure CO to syngas ($H_2/CO=1$) as a function of temperature (a- Fe/SiO_2, b- $FeSn/SiO_2$; c- $FeSb/SiO_2$, d- $SbFe/SiO_2$).

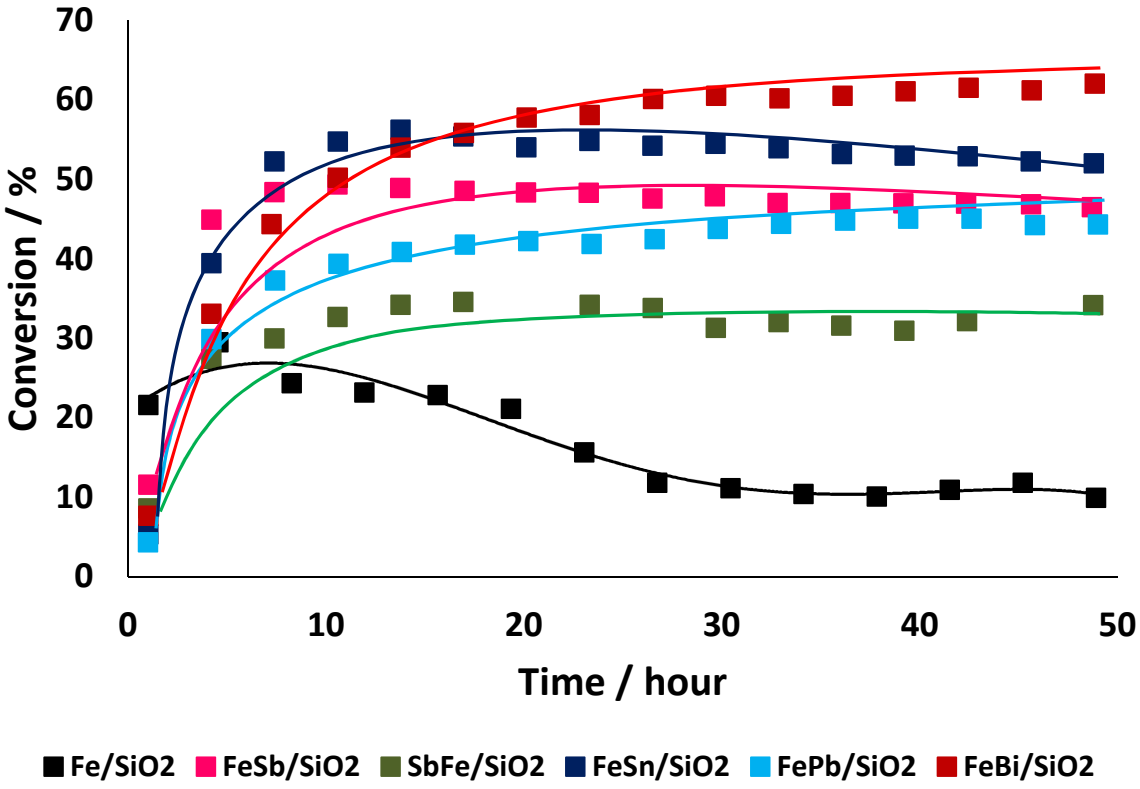

Figure 8. CO conversion as a function of time for iron catalysts promoted with Sn, Sn, Bi and Pb. Reaction conditions: P = 10 bar, H_2/CO = 1, WHSV = 3.6 L g^{-1} h^{-1}.

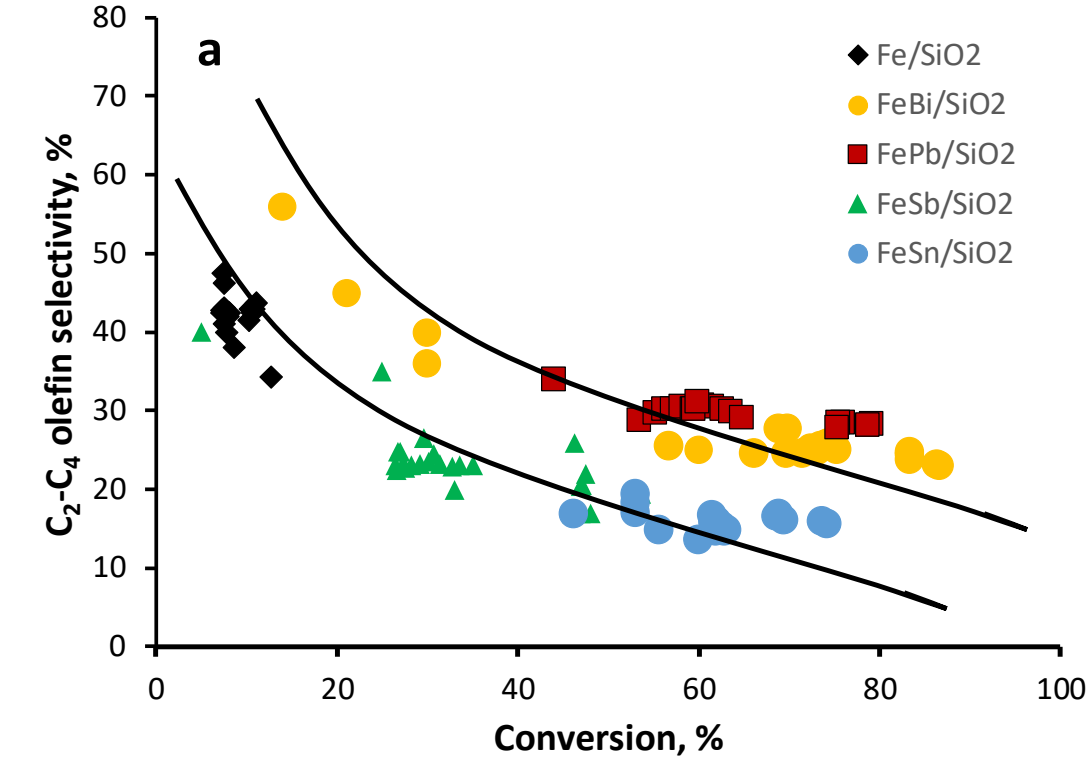
a
Fe/SiO2
FeBi/SiO2
FePb/SiO2
FeSb/SiO2
FeSn/SiO2
C2-C4 olefin selectivity, %
Conversion, %
0
10
20
30
40
50
60
70
80
0
20
40
60
80
100

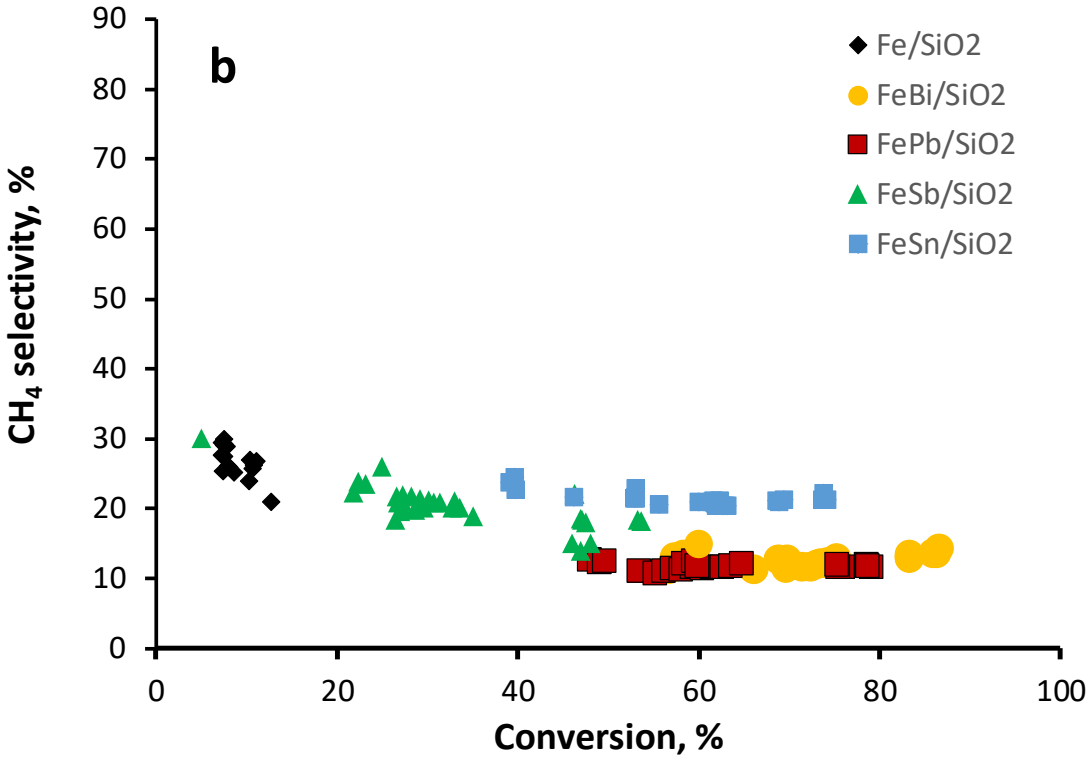
b
Fe/SiO2
FeBi/SiO2
FePb/SiO2
FeSb/SiO2
FeSn/SiO2
CH4 selectivity, %
Conversion, %
0
10
20
30
40
50
60
70
80
90
0
20
40
60
80
100

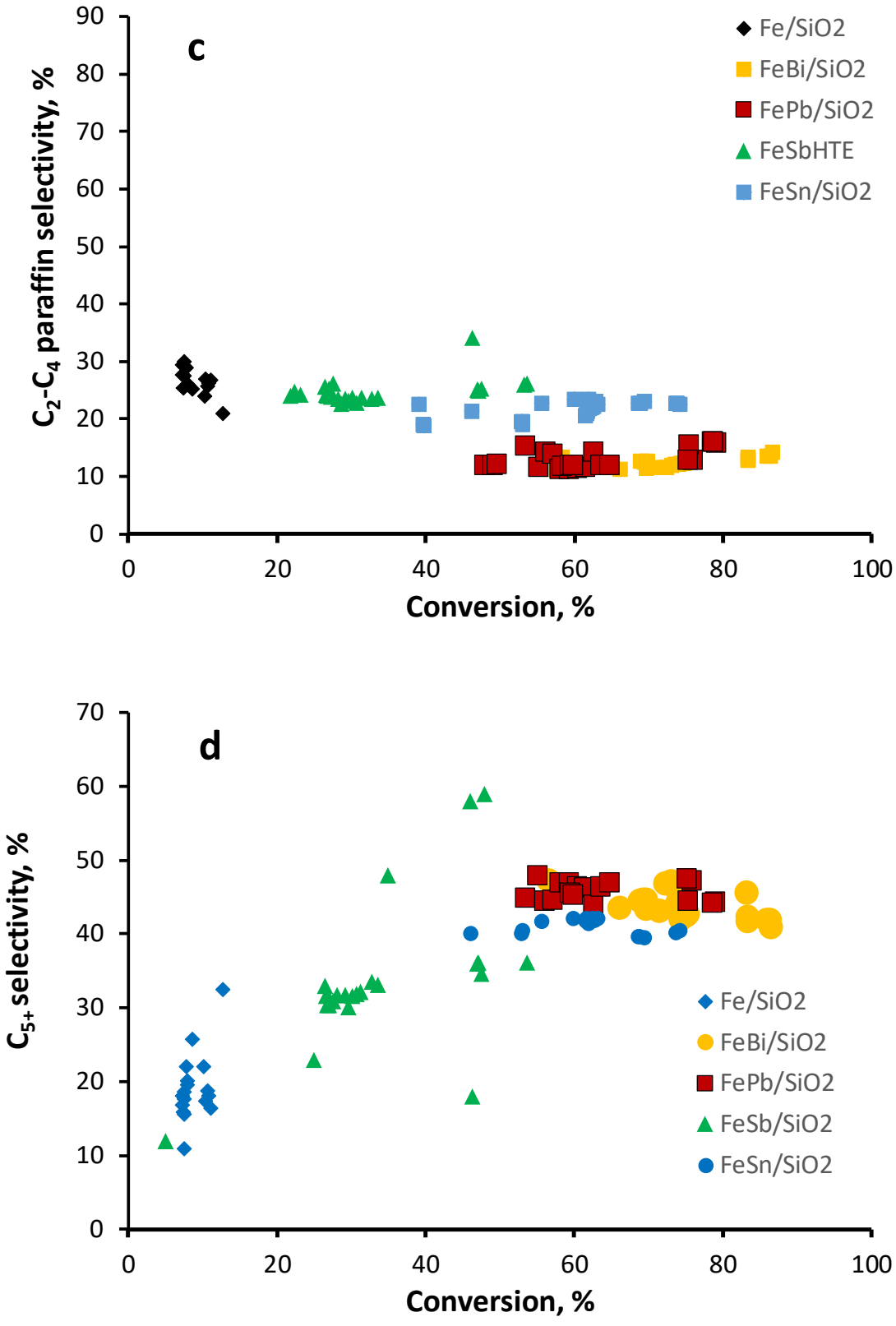

Figure 9. Selectivity-conversion curves for silica supported iron catalysts promoted with Bi, Pb, Sn, Sb and reference iron catalysts.

Table 1. Physical properties of supported Fe catalysts.

Sample	Fe content[a] (wt%)	Promoter content[a] (wt%)	D_{oxide}[b] (nm)	Total H_2 consum[c] (mmol/g)
Fe/SiO_2	11.2	-	17	2.76
$FeBi/SiO_2$	10.8	0.75	15	2.81
$FePb/SiO_2$	11.9	0.79	17	2.68
$FeSn/SiO_2$	10.9	0.69	11	2.77
$FeSb/SiO_2$	9.4	0.72	22	2.70
$SbFe/SiO_2$	11.0	0.78	16	2.62

[a]The Fe and promoter content from XRF.

[b]Average particle size of iron oxide by XRD.

[c]The total H_2 consumption and iron reducibility degree from TPR analysis.

Table 2. Catalytic performance of iron catalysts promoted with soldering metals in FT synthesis measured in a conventional fixed bed reactor at iso-GHSV (10 bar, 350 °C, H_2/CO = 1/1, WHSV = 3.6 L/g.h, TOS = 48h)

Catalysts	FTY 10^{-4} $mol_{CO}g_{Fe}^{-1}s^{-1}$	TOF, s^{-1}	CO conv. (%)	CO_2 select. (%)	Hydrocarbon selectivity (%)				$C_{2-4}^{=}/C_{2-4}^{o}$
					CH_4	$C_{2-4}^{=}$	C_{2-4}^{0}	C_5^{+}	
Fe/SiO_2	0.20	0.059	11	15	24	31	5	40	6.20
$FeBi/SiO_2$	1.11	0.110	60	49	15	25	10	50	2.50
$FePb/SiO_2$	0.82	0.122	44	46	16	34	7	43	4.86
$FeSn/SiO_2$	0.98	0.122	53	49	23	17	13	47	1.31
$FeSb/SiO_2$	0.87	0.108	47	47	14	17	10	59	1.70
$SbFe/SiO_2$	0.61	0.091	33	43	21	20	12	47	1.67

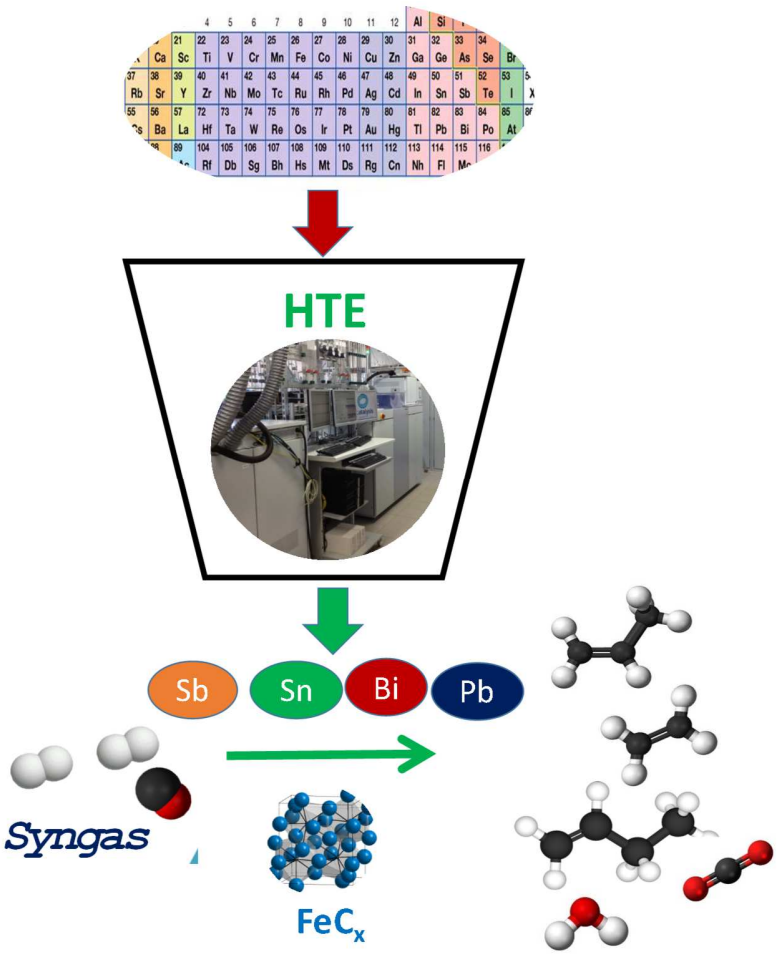
HTE
Sb
Sn
Bi
Pb
Syngas
FeCx